Norwegian University of
Science and Technology

Comparing diffraction from industry and transportation using NORD96, CNOSSOS-EU and NORD2000

Jan Arne Almeland Bosnes

Supervisor: Prof. Guillaume Dutilleux, IES
Co-supervisor: Ingunn Milford and Jens Holger Rindel, Multiconsult

Master of Science in Electronics
Submission date: June 16, 2019
Norwegian University of Science and Techology
Faculty of Information Technology and Electronics

Problem Description

When calculating noise maps for evaluating noise pollution on communities from noise sources, such as industry and road traffic, accurately predicting the attenuation from diffraction is a vital aspect. This master thesis will compare both single-edge and double-edge diffraction from different prediction methods and compare them to field measurement at ideal locations and in favourable conditions.

Abstract

This master's thesis compares three noise prediction methods focusing on diffraction by a single-edge and a double-edge barrier, from road traffic and industrial noise. The three methods are the Nordic prediction method from 1996 (NORD96), the new standard European method (CNOSSOS-EU), and the Nordic prediction method from 2000 (NORD2000). The predicted values are compared from two diffraction measurements from two barriers. One was a screen, and another was a building that represented the single-edge and double-edge barrier, respectively.

Comparing the sound pressure level and the continuous equivalent sound level between the field measurements and the prediction method, CNOSSOS-EU on average, gives more accurate predictions. NORD96 seem to give acceptable results on single-edge diffraction but had clear discrepancies at double-edge diffraction. Finally, NORD2000 gave, in general, a lower sound pressure level compared to measured results.

This thesis contributes to a topic which requires further research and to obtain more reliable results; several improvements can be made.

Sammendrag

Denne mastergraden sammenligner tre støyprediksjonsmetoder som fokuserer på diffraksjon med en enkelkants- og en dobbelkantsbarriere fra trafikk og industriell støy. De tre prediksjonsmetodene er den nordiske metoden fra 1996 (NORD96), den nye europeiske metoden (CNOSSOS-EU) og den nordiske metoden fra 2000 (NORD2000). De beregnede verdiene sammenlignes med diffraksjonsmålinger ved to barrierer. Det ene barrieren var en støyskjerm, og den andre var en bygning som henholdsvis gjenga enkelkants- og dobbelkantsdiffraksjon.

Sammenlignet med lydtrykknivået og det kontinuerlige ekvivalente lydnivået mellom feltmålinger gir CNOSSOS-EU i gjennomsnitt mer nøyaktige beregninger. NORD96 ser ut til å gi akseptable resultater på enkelkantsdiffraksjon, men hadde tydelige avvik ved dobbeltkantsdiffraksjon. NORD2000 ga generelt et lavere lydtrykknivå sammenlignet med målte resultater.

Denne oppgaven bidrar til et felt som trenger videre forskning og for å oppnå mer pålitelig resultater, er det flere forbedringer som kan gjøres.

Acknowledgements

This master's thesis is the final work on my master's degree in acoustics at the Norwegian University of Science and Technology. The project was proposed by Multiconsult, and the physical measurements were carried out by the author and Multiconsult in Oslo. The Department of Electronic Systems has collaborated with theoretical support.

I would like to thank Multiconsult for the help I received when I was conducting the measurements as well as giving me technical support on the simulations.

These people working at Multiconsult deserves special thanks:

- Ingunn Milford for initiating the project and putting in the resources necessary for finishing my research.
- Jens Holger Rindel for providing his knowledge and for giving me important feedback on the results.
- Henrik Lødrup Parnemann for the support when I conducted the measurements and implemented the simulations.

Furthermore, I would like to express my gratitude to my supervisor Prof. Guillaume Dutilleux for excellent guidance, advice and helpful discussions throughout the entire project.

I wish to thank Herold Olsen for feedback on topics regarding NORD2000. Also, a special thank to my peer-students Andreas Sæle, Live Østvik, Per Christian Olafsson and Malene Monslaup for their feedback regarding my results.

Contents

List of Figures

List of Tables

Chapter 1

Introduction

Noise pollution is a genuine problem in modern cities. It has been found that long term exposure to high levels of sound has an indirect impact on productivity and is the main contributor to sleep deprivation [1]. It is essential to accommodate the noisy city environment by designing it in a way that ensures sufficient protection against any damaging exposure. One way of protecting against noise pollution is by shielding the noise source with a construction avoiding any propagation in direct line of sight of the listener. As illustrated in figure 1.1 this can be intentional by placing a screen between a noise source such as road traffic (figure 1.1a), or it can be incidental where a building is shielding the recipient from the noise source (figure 1.1b). The sound would then bend and travel along edges, which is a physical phenomenon called diffraction [2]. Diffraction can be a crucial factor in reducing noise and is the phenomena that will be studied in this thesis.

(a) (b)

Figure 1.1: Illustration of noise barriers such as a single screen (a) and a building (b).

In recent years, there has been considerable interest in studying how precise noise predictions are possible to make and which prediction model is the most accurate. In Norway, the Ministry of Climate and Environment published a directive [3] in 2016 with guidelines aimed at arranging long term disposal that would prevent damaging noise levels and allow for a logical approach rooted in professional evaluation of the attenuation of environmental noise. The guidelines focus specifically on suggesting how to establish noise protected areas and include recommendations on how to map noise sources such as road and industry, and it has been addressed to the local authority where there has been a need for noise mapping of cities to review areas that are suspected of having high exposure to noise pollution. According to the directive T1442/2016 [3], a source in an area which is not suited for noise sensitive purposes, e.g. hospitals (noted as red zones), has an upper day-evening-night sound limit (L_{den}) of 65 dB for road traffic and industry

noise[1]. Areas that are subjected to a noisy environment, but can have noise sensitive uses so long as precautions are made to ensure satisfactory noise levels (yellow zones), must have an upper L_{den} limit of 55 dB[2]. Research is necessary to affirm that the cities have met these criteria. Especially mapping yellow zones that can be approved by implementing screens or other forms of noise damping. Such research is dependent on reliable methods where there is a consensus in the academic and acoustic communities on which methods are most accurate and preferable. Multiconsult contributes to research comparing prediction methods after a directive from the European Union (EU) has member countries adopting a new prediction method. It is not yet decided if this method only is to be used for overall mapping or if it is suitable for more accurate calculations as well.

The thesis compares three prediction models with a focus on diffraction. Most of the theory are retrieved from the following references:

- **NORD96** The Nordic prediction model from 1996 is elaborated on the report from the Danish Environmental Department [4]. It is a fairly old method, and parts of it are rooted in empirical data made from experiments. It might be a disadvantage since the model can predict incorrect results in certain situations, and there has been a demand for standardizing a more accurate method.

- **CNOSSOS-EU** The EU's official journal [5] describes in detail the common noise assessment methodical framework in the European Union. CNOSSOS-EU launched in 2008 and is based upon the French standard for road traffic noise (NMPB-2008). The guidelines of this project became relevant when the Commission Directive (EU) voted it into effect in 2015 were article 2 part 1 states that all the member states were to adopt the new standard within December 31th 2018. The directive does not only include noise from transportation such as road traffic, railway and aerospace but also has guidelines for noise prediction from industries. CNOSSOS-EU is a direct copy of the French method for noise prediction (NMBP-2008) and has been common in France mainly for predicting road traffic noise.

- **NORD2000** The Nordic prediction model from 2000 is explained in detail from its report that was made by Danish Electronics, Light and Acoustics (DELTA) and revised in January 2014 [6]. NORD2000 is a noise mapping method created with the cooperation between academic communities in the Nordic countries. It is mainly built on theoretical models and regarded as one of the complicated methods due to all the variables that it takes into account. Among those, are many weather variables, which is not that prominent in the other methods. It makes it much more demanding in terms of processing power, time consumption and requirements of the input data.

This thesis will try to reveal critical differences between the prediction methods focusing on diffraction and ground attenuation. Measurements will be conducted on one and double edge configurations at close range with a controlled source and compared with simulations using the prediction methods implemented in SoundPlan 8.0.

Structure

The structure of the thesis is as follows: chapter 2 will present the basics of ground effect and diffraction and go then go on introducing the different prediction methods. The main basis

[1]For industry noise, L_{den} have different limits of 60 dB and 65 dB regarding industries with and without impulse noise respectively.

[2]For industry noise, L_{den} have different limits of 50 dB and 55 dB regarding industries with and without impulse noise respectively.

of the chapter explains how the individual methods model ground attenuation and diffraction. Then chapter 3 will elaborate on the practical measurement and computer simulations. The results will be illustrated in chapter 4 and discussed in chapter 5. Finally, in chapter 6 the conclusion will sum up the main findings in this thesis, addressing any topics regarding improvements and further work.

Chapter 2

Theoretical Background

This chapter presents the theoretical background behind each prediction method but also introduces the concept of diffraction and ground attenuation. First, some basic concepts are presented where two textbooks; *The Science of Sound* by Rossing et Al. [7] and *Building Acoustics* by Vigran [8] are references. Then, the principle of diffraction is described with lecture notes from Rindel [2] with the author's permission. The definition of the image source method is taken from a paper by Allen and Berkely [9], Hadden and Pierce [10] define wedge diffraction, and an impedance model is presented using a paper from Delany and Bazely [11]. The thesis will only study diffraction in near-field and also when the edge of the occurring diffraction is higher than the receiver and the source so that there is no direct line of sight between them. Also, meteorological factors are considered to be out of the scope of this thesis. Some theoretical knowledge is assumed known by the reader, including knowledge about the Heaviside-function and the Signum-function.

2.1 Sound Pressure Level and Sound Power Level

As defined by [7], the sound pressure is found in Pascal [Pa]. For comparing two quantities, the decibel scale is used when expressing sound according to the perception of the human ear.

$$L_p = 20 \log \frac{p}{p_0} \tag{2.1}$$

Where $p_0 = 2 \cdot 10^{-5}$ Pa is the amplitude of the ear threshold audibility at a frequency of 1 kHz, the sound pressure level, L_p is from now on referred to as the SPL.

Sound power is a measure of the total emitted energy per unit time [8]. The source has a constant sound power that does not change if it is placed in a different room environment and is a theoretical value expressed in Watts [W].

$$L_W = 10 \log \frac{W}{W_0} \tag{2.2}$$

Eq. 2.2 express the sound power level L_W, also referred to as SWL, is the logarithmic measure of the sound power relative to the reference power $W_0 = 10^{-12}$ W, which is the lower threshold of the human ear.

2.2 Summation, A-Weighting and Continuous Average Sound Pressure Level

The energy summation for noise levels is simplified by denoting $\oplus$ as described in [6].

$$L_1 \oplus L_2 = 10\log_{10}\left(10^{(L_1/10)} + 10^{(L_2/10)}\right) \tag{2.3}$$

where L_1 and L_2 are arbitrary sound levels.

A-weighting is a correction of the SPL by introducing a roll-off at low-frequencies to further resemble the response of the human ear. The correction factor at each octave band presented in the table 2.1. The following equation was used to find the correction for A-weighting SPL at each octave band [12]:

$$R_A(f) = \frac{12194^2 f_b^4}{(f_b^2 + 20.6^2)\sqrt{(f_b^2 + 107.7^2)(f_b^2 + 737.9^2)}(f_b^2 + 12194^2)}$$

Where f_b is the octave band frequency. Converting this into dB as shown,

$$A(f) = 20\log_{10}(R_A(f)) + 2$$

we get a correction factor for each octave band frequency presented in table 2.1.

A - weighted correction factor								
Octave band frequency f_b [Hz]	63	125	250	500	1000	2000	4000	8000
Computed correction [dB]	-26.2	-16.2	-8.7	-3.2	0.0	1.2	1.0	-1.1

Table 2.1: A-weighted level at each octave band.

The next step is to A-weight the SPL, L, at each octave band by adding the correcting factor.

$$L_A = [L_{63} + A_{63}, L_{125} + A_{125}, ..., L_{8000} + A_{8000}]$$

Which lead to the final computation of $L_{A,eq}$.

$$L_{A,eq} = L_{A,63} \oplus L_{A,125} \oplus ... \oplus L_{A,8000} = 10\log_{10}\left(\sum_{i=1}^{8} 10^{((L_i + A_i)/10)}\right) \tag{2.4}$$

where i in eq. 2.4 denotes the frequency bands index from table 2.1, and A_i and L_i being the A-weighted correction factor and the SPL of that certain octave band, respectively.

As defined in [5], the Continuos A-weighted Average Sound Pressure Level $L_{A,eq}$ is found by summing all frequency bands. The thesis considers bands frequency from 63 Hz to 8 kHz to be relevant, thus having 8-octave bands that are A-weighted and summed.

2.3 Ground Effect

As defined in [5], the attenuation due to interference between the direct wave and the waves reflected from a surface with specific porosity is referred to as the ground effect.

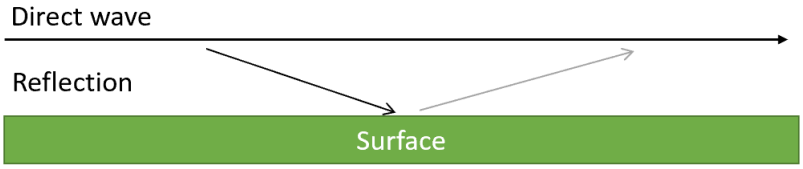

Figure 2.1: Illustration of the ground effect across different surfaces.

Figure 2.1 illustrates that the wavefront may travel along a surface categorized as *soft*, *hard*, or a combination of those two depending on the prediction model. A soft surface has a specific absorption that weakens the reflections so that the impact on the direct wave is low compared to a hard surface that has no absorption and thus emits the reflected wave with the same energy as the incident wave.

2.4 Diffraction

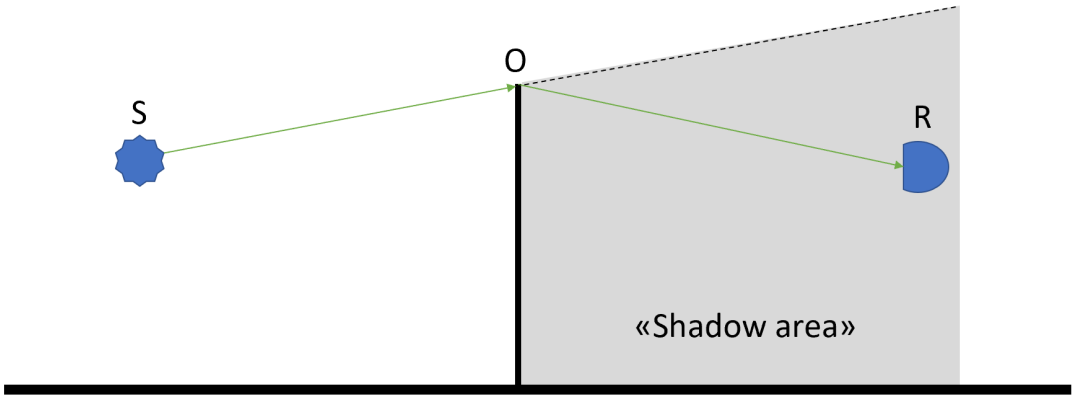

Figure 2.2: Illustration of diffraction from a single screen marking the shadow area.

Diffraction is the bending or deflection of waves when sound propagates around an obstacle edge. It is especially essential when the noise barrier is used to create a so-called *shadow area*, as illustrated in figure 2.2. The assumption is that the barrier is a thin screen with a hard surface where the transmission of the sound through the screen is negligible. According to to [2], there are many different theories on diffraction. Most of them are mere approximations that are adapted to various forms of applications. What most prediction methods seem to imply is that diffraction is a combination of unobstructed incident waves that interfere in a superposition with scattered waves by the edge. Diffraction can also occur along flat surfaces with an impedance discontinuity. There is still ongoing research on diffraction, especially which method most realistically describes the behaviour of the sound waves within the shadow area.

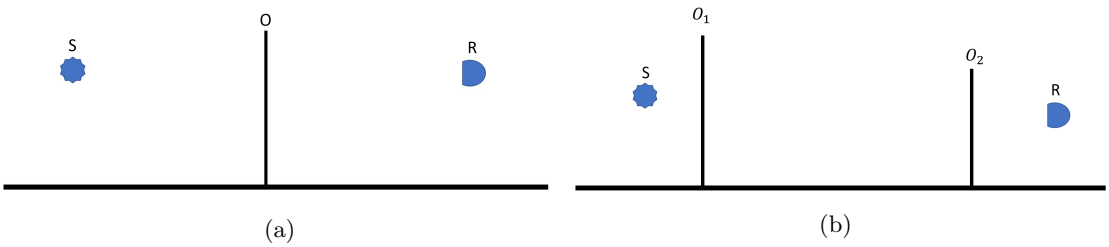

(a) (b)

Figure 2.3: Single screen (a) and double screen configuration (b).

Diffraction is an essential concept since screens are the go-to solution for shielding against noise from highway, railway or airport. When designing noise barriers, it is a compelling interest to have schemes that accurately predicts the sound reduction. This thesis will focus on diffraction of the direct line with a source S emitting sound to a receiver R between a single screen and a double screen configuration as illustrated in figure 2.3a and 2.3b respectively. Studying only 2D-illustrations any impact from side diffraction is considered negligible. Even though it is an essential factor, it is considered out topic.

2.5 NORD96

2.5.1 Computing the Sound Pressure Level

NORD96 relies on both theoretical and empirical formulae, the last being especially true for ground attenuation. The prediction method adds point sources that measure sound power level, L_W, at 1/1-octave band between 63 Hz and 8kHz. When considering the transmission path between the source and receiver and finding the sound pressure level at the receiver, $L_{W,r}$, a correction variable consisting of several geometrical and environmental factors, ΔL, is subtracted from the source power in eq. 2.5:

$$L_{W,r} = L_W - \Delta L \tag{2.5}$$

The correction variable is further divided into seven different factors, as shown in eq. 2.6:

$$\Delta L = \Delta L_d + \Delta L_a + \Delta L_r + \Delta L_s + \Delta L_v + \Delta L_i + \Delta L_g \tag{2.6}$$

Here, ΔL_d, ΔL_a, ΔL_r, ΔL_v, and ΔL_i, are the attenuations from the distance, air absorption, side reflections, vegetation, and internal spreading, respectively. These will not be studied further since they are not within the scope of this thesis. ΔL_g is the attenuation from the ground effect which will be further elaborated in section 2.5.2 and ΔL_s is the attenuations from diffraction which will be discussed in 2.5.3.

2.5.2 Ground Attenuation

When computing the ground attenuation, the N96 model is most accurate on surfaces such as asphalt, water, and terrain with many obstacles that diffuse the sound radiation [4]. These are defined as *hard* surfaces. The model is also accurate on surfaces prone to vegetation, and where few obstacles diffuse the sound rays. Such surfaces include lawns and grass fields, both agricultural and suburban, as well as areas of varying vegetation. These kinds of terrain are referred to as soft surfaces. The model is less accurate when it comes to terrain that has both soft and hard surface properties, such as dirt roads and gravel fields. For such terrain, an interpolation using the ground value G, is used [4]. The coefficient can either be 0 or 1, specifying the terrain as hard or soft respectively. The application of the ground coefficient is shown in appendix B.

The attenuation ΔL_g of the ground is defined by three correction factors shown in the following equation:

$$\Delta L_g = \Delta L_{g,s} + \Delta L_{g,r} + \Delta L_{g,c} \tag{2.7}$$

Here, $\Delta L_{g,s}$ specifies the ground attenuation at the source and $\Delta L_{g,r}$ is the ground attenuation at the receiver. $\Delta L_{g,c}$ is the ground attenuation between the source and the receiver, referred to as the *center* or interpolation area, and is only valid when the distance between source and receiver exceeds a specified limit. The correction factors depend on the frequency, character and terrain. For hard terrain surfaces, the correction factors would always be higher or equal to 0 dB. For soft terrain, the correction factors are always less than, or equal to 0 dB, except for the 63 Hz-octave. The empirical expressions for the ground effect in each octave band is found in appendix B.

2.5.3 Diffraction

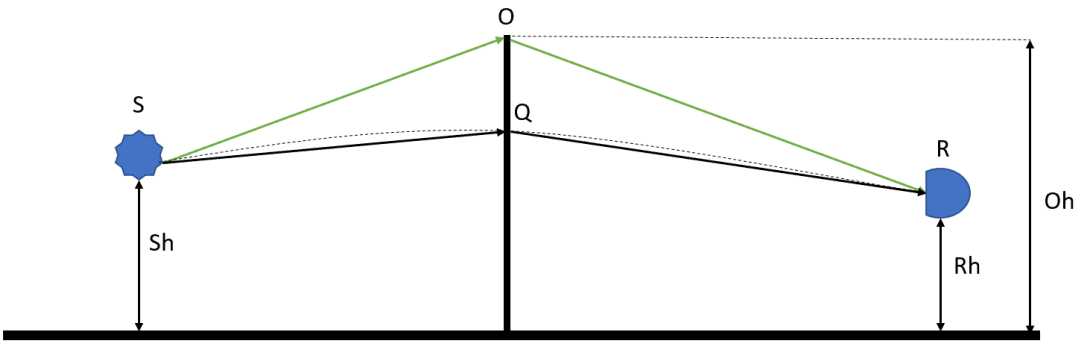

Figure 2.4: Simplified illustration of screening effect.

The attenuation of the screening properties is equivalent to the same as the impact diffraction has on the propagation, as shown in figure 2.4. Here the illustration shows the effect of one screen between source S and receiver R. The altered paths from source to the edge of the obstacle O and the receiver are compared with the propagation path the sound would have, through the intersection point on the screen Q. This direct path is adapted to represents an almost circular path (shown with a dashed line) and represent the projection in *favorable* conditions where downward refraction is present. Since no side diffraction the screen is considered, one will obtain a simplified equation of the diffraction as described [4]:

$$\begin{cases} \Delta L_s = 0 & \text{for } N_v \leq -0.1 \\ \Delta L_s = 10 \cdot C_h \cdot \log_{10} \frac{1}{20N_v+3} & \text{for } N_v \geq -0.1 \end{cases} \tag{2.8}$$

If ΔL_s is below -20 dB, then -20 dB is used and above 0 dB, 0 dB is used. C_h in equation 2.8 is a correction to prevent low screens from having too much of an attenuation. It is expressed as:

$$C_h = \frac{f_c}{250} \cdot Oh \tag{2.9}$$

where f_c is the centre frequency and Oh is the screen height. N_v is a correction of the centre frequency and the path difference, δ_v:

$$N_v = 0.0047\delta_v \cdot f_c \tag{2.10}$$

Here δ_v is found by taking the sum of the ray paths of the screen edge and subtract it from the projected path when no screen is present.

$$\delta_v = |SO| + |OR| - |SQ| - |QR| \tag{2.11}$$

Where $|SO|$ represents the path length from the source to the top edge of the screen and so on. The formula is a simplified version of the ideal case from [4].

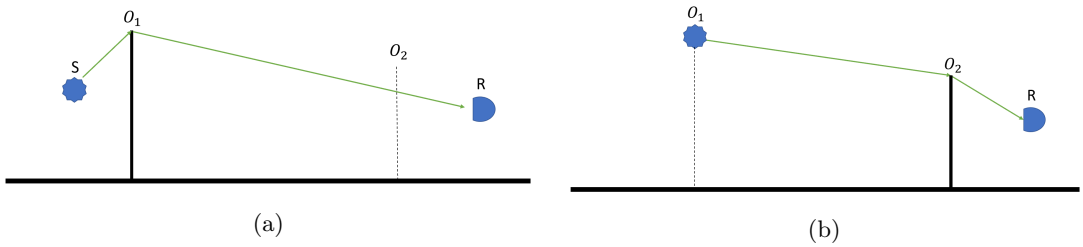

Figure 2.5: Diffraction on screen 1 (a) and diffraction on screen 2 (b).

Figure 2.5 shows how a double-screen configuration is computed. When there is more than one screen affecting the sound propagation, the total attenuation is summed as independent single-screen configurations. First, as illustrated in figure 2.5a, the diffraction on the first screen is found as if there is no second screen in between the source and receiver. Then as illustrated in figure 2.5b, the diffraction on the second screen is found by placing the source at the top of the first screen and computing the diffraction from the altered position. The total attenuation of the screens $\Delta L_{2screens}$ is found as follows:

$$\Delta L_{2screens} = \Delta L_{s1} + \Delta L_{s2} \tag{2.12}$$

whereΔL_{s1} and ΔL_{s2} are the attenuations from screen 1 and 2 respectively.

2.6 CNOSSOS-EU

The sound pressure level at the receiver point L_R is determined by the directional sound power level $L_{W,dir}$ of a point source S and the attenuation A expressed as follows:

$$L_R = L_{W,dir} - A \tag{2.13}$$

In eq. 2.13 the attenuation is the sum of the attenuation due to the atmospheric absorption A_{atm}, the attenuation due to the geometrical divergence A_{div}, and the attenuation due to the boundary of the propagation in the medium $A_{boundary}$.

$$A = A_{div} + A_{atm} + A_{boundary} \tag{2.14}$$

The attenuation from the propagation boundary has two considerations. Firstly, the propagation path with no obstacles is determined (assuming negligible diffraction) so we only compute the ground effect, meaning $A_{boundary} = A_{ground}$. If one considers a path with obstacles, the path attenuation will be set, $A_{boundary} = A_{diff}$. A_{diff} also takes the ground effect into account. Secondly, one must also consider homogenous and favourable conditions. Since the measurements are conducted at close range, the assumption is that homogenous conditions are present[1]. All these considerations are presented in table 2.2. The noise is evaluated for between 63 Hz and 8 kHz at 1/1-octave bands.

The image source method for rigid surfaces is a practical method to study the specular reflections. CNOSSOS-EU uses the image source method to determine the reflections from the source and the receiver. It is a known method in room acoustics, and further elaboration can be found in [9].

	Ground effect only	**Ground effect with diffraction**
Homogenous	$A_{ground,H}$	$A_{diff,H}$
Favorable	$A_{ground,F}$	$A_{diff,F}$

Table 2.2: Attenuation from propagation medium $A_{boundary}$.

2.6.1 Ground Attenuation

For a single screen configuration as in figure 2.3a in near field, the ground effect on the source side $\Delta_{ground,SO}$ and the ground effect on the receiver side, $\Delta_{ground,OR}$. We must first compute the ground coefficient G_{path} which depends on the ground value G chosen from table B.2 appendix B and computing the mean ground plane d_p using the ground plane of the source d_1 and the ground plane of the receiver d_2 as follows:

$$d_p = d_1 + d_2 \tag{2.15}$$

The ground coefficient is given by:

$$G_{path} = \frac{G_s \cdot d_1 + G_r \cdot d_2}{d_p} \tag{2.16}$$

Eq. 2.16, where G_s and G_r are the ground values of the ground beneath the source and receiver respectively, is then determined depending on the distance between the source and the

[1]For further details regarding attenuation under favourable conditions, see [5].

receiver. The equivalent source, z_s and receiver positions, z_r is used to compute a corrected ground factor G'_{path}. If $d_p \leq 30(z_s + z_r)$, then we get the following:

$$G'_{path} = G_{path}\frac{d_p}{30(z_s + z_r)} + G_s(1 - \frac{d_p}{30(z_s + z_r)}) \tag{2.17}$$

The ground factor and the corrected ground factor determine generic notations G_w and G_m. G_w is determined by given equations A.1 from the appendix. With $G_{path} \neq 0$, meaning ground absorption is present, the attenuation is determined by:

$$A_{ground,H} = max\left(-10\log_{10}\left[4\frac{k^2}{d_p^2}(z_s^2 - \sqrt{\frac{2C_f}{k}}z_s + \frac{C_f}{k})(z_r^2 - \sqrt{\frac{2C_f}{k}}z_r + \frac{C_f}{k})\right], -3(1 - G_m)\right) \tag{2.18}$$

Where $k = 2\pi f_m/c$, where f_m is the center frequency of the frequency band and C_f is determined in equation A.1 which can be found in Appendix A.

Finally, we can express the ground attenuations eq. 2.19 and 2.20 which will be put into eq. 2.22.

$$\Delta_{ground,SO} = -20\log_{10}\left(1 + \left(10^{-(A_{ground,SO})/20} - 1\right)10^{-(\Delta_{diff,S'R} - \Delta_{diff,SR})/20}\right) \tag{2.19}$$

$$\Delta_{ground,OR} = -20\log_{10}\left(1 + \left(10^{-(A_{ground,OR})/20} - 1\right)10^{-(\Delta_{diff,SR'} - \Delta_{diff,SR})/20}\right) \tag{2.20}$$

Here $\Delta_{diff,SR}$, $\Delta_{diff,S'R}$ and $\Delta_{diff,SR.}$ are formulas for determining the diffraction. They will be explained in section 2.6.2.

2.6.2 Diffraction

With the image source model, as illustrated in figure 2.6, CNOSSOS-EU use geometrical diffraction theory since both source and receiver are predefined. The method for finding the SPL is grounded in the concept of the propagation path. The shape and size of topography and obstacles determine the paths.

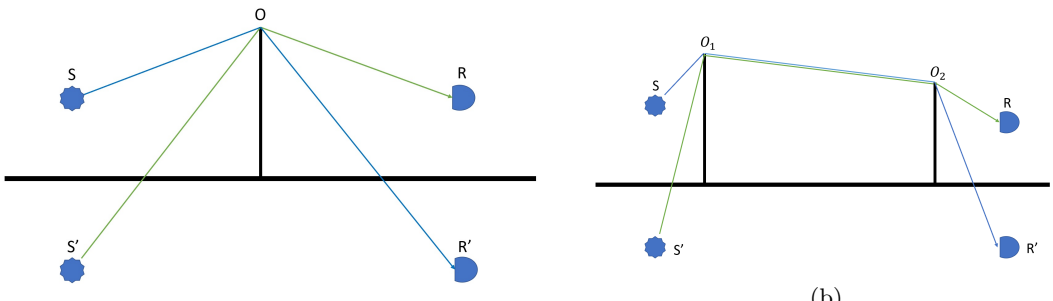

Figure 2.6: Diffraction by image sources of a single screen (a) and a double screen configuration (b).

As indicated in figure 2.6a three diffractions are computed, first is the direct line from the source to the obstacle edge O to the receiver $\Delta_{diff,SR}$, then from the image source to the receiver $\Delta_{diff,S'R}$ and finally, from the source to the image receiver $\Delta_{diff,SR'}$:

$$\Delta_{diff} = \begin{cases} 10 \cdot \log_{10}(3 + (40/\lambda)C''\delta) & \text{if } (40/\lambda)C''\delta \leq -2 \\ 0 & \text{otherwise} \end{cases} \tag{2.21}$$

Where λ is the wavelength at the nominal centre frequency of considered frequency band and δ is the path difference between the diffraction path and the direct path. C'' is a coefficient used to take into account multiple diffractions as illustrated in figure 2.6b. For multiple diffractions C'' is redefined in eq. A.1 in appendix A. Δ_{diff} is bounded, meaning the minimum value is 0 dB and the maximum value is 25 dB.

The path difference is computed with reference to figure 2.6a and 2.6b.

- $\delta_{SR} = |SO| + |OR| - |SR|$ for a single diffraction and $|SO_1| + |O_1O_2| - |O_2R|$ for double diffraction.
- $\delta_{S'R} = |S'O| + |OR| - |S'R|$
- $\delta_{SR'} = |SO| + |OR'| - |SR'|$

The attenuation can then be found by equation 2.22:

$$A_{diff} = \Delta_{diff,SR} + \Delta_{ground,SO} + \Delta_{ground,OR} \tag{2.22}$$

$\Delta_{ground,SO}$ and $\Delta_{ground,OR}$ are the attenuations due to the ground effect between the source S and diffraction point O, and between the diffraction point O and the receiver R respectively.

2.7 NORD2000

The Nordic prediction method or NORD2000 is by far the most advanced prediction method described in this thesis. NORD2000 can predict diffraction from noise barriers of different types in complex terrain. The method is mostly theoretical, and it is more complicated to use since it requires a large number of input parameters, and it tends to be demanding both in time and processing power. According to [6], NORD2000 predicts environmental noise from roads, railways, industrial plants, as well as air traffic. For industry and road traffic, noise is predicted at one-third octave band from 25 Hz to 10 kHz propagating from a point source to a receiver within a range of 1 km.

A two-dimensional terrain profile is considered and approximated by several straight line segments. Various structures, including screens, have been made part of the terrain profile. Similar to the other prediction methods, auxiliary functions describing attenuations from different outdoor factors are added to the sound radiating from the source. In NORD2000, this is expressed in equation 2.23.

$$L_R = L_w + \Delta L_d + \Delta L_a + \Delta L_t + \Delta L_s + \Delta L_r \tag{2.23}$$

L_w is the SWL, $\Delta L_a, \Delta L_t, \Delta L_s$ and ΔL_r the propagation effect from divergence ΔL_d, the effect of air absorption ΔL_a, the effect of the terrain ΔL_t, the effect of the scattering zones ΔL_s and the effects from reflections ΔL_r. Most of these propagation effect will not be studied further. This thesis will focus on ΔL_t where the attenuation of the terrain is a combination between ground effect and diffraction obstacles.

2.7.1 Ground Impedance

Unlike NORD96 and CNOSSOS-EU, the ground value G is not determined in NORD2000. Instead, the terrain surface is described by the Delany-Bazely impedance model defined in equation 2.24 which is an empirical formula for homogenous and isotropic fibrous materials. These are then normalized into a dimensionless group [11].

$$\hat{Z_G}(f_m) = 1 + 9.09\left(\frac{1000 f_m}{\sigma}\right)^{-0.75} + j11.9\left(\frac{1000 f_m}{\sigma}\right)^{-0.73} \tag{2.24}$$

The complex expression of the impedance expressed by the middle frequency at each octave band f_m and the flow resistivity σ which is determined from table B.3 in appendix B.

2.7.2 Diffraction

Single edge diffraction

According to [6], finding the complex diffraction attenuation $\hat{p}_{diffr}(f)$ given a wedge with finite impedance, the SPL at the receiver R is expressed with equation 2.25 using the variables shown in 2.7.

$$\hat{p}_{diffr}(f) = -\frac{1}{\pi}\sum_{n=1}^{4} \hat{Q}_n A(\theta_n)\hat{E}_v(A(\theta_n))\frac{e^{j\omega\tau}}{l} \tag{2.25}$$

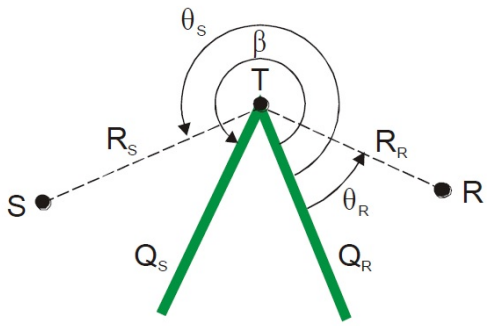

Figure 2.7: Illustration of diffraction on a wedge with finite impedance showing necessary variables for eq. 2.25 [6].

Here $\omega = 2\pi f$ is the angular frequency, τ is the time for the sound to travel from the source S via the wedge edge T to the receiver R and l is the length of the direct line with the same path as τ. Four angles are found as follows:

$$\begin{aligned}\theta_1 &= \theta_S - \theta_R \\ \theta_2 &= \theta_S + \theta_R \\ \theta_3 &= 2\beta - \theta_2 \\ \theta_4 &= 2\beta - \theta_1\end{aligned} \tag{2.26}$$

The reflection coefficients, $\hat{Q}_n$ are then found as follows:

$$\begin{aligned}\hat{Q}_1 &= 1 \\ \hat{Q}_2 &= \hat{Q}_S \\ \hat{Q}_3 &= \hat{Q}_R \\ \hat{Q}_4 &= \hat{Q}_S\hat{Q}_R\end{aligned} \tag{2.27}$$

$\hat{E}_v(A(\theta_n))$ is a help-function that combines the computation of the Heaviside-function, the Signum-function and, most importantly, the fresnel-function which is found using polynomial fit. Also, $v = \pi/\beta$ is denoted as the wedge index. As it is quite complicated calculus, these will not be further elaborated.

The diffraction coefficient is found as follows:

$$\hat{D}(f) = \hat{p}_{diff}(f)\frac{e^{j\omega\tau}}{l} \tag{2.28}$$

Double edge diffraction

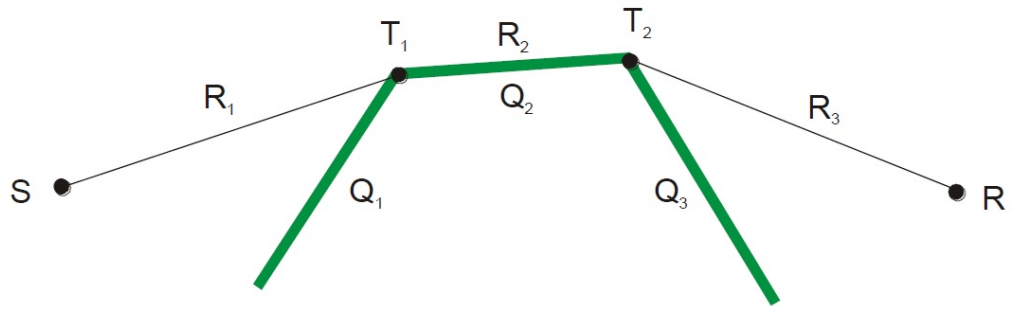

Figure 2.8: Thick screen configuration [6].

The closest configuration of a double edge diffraction by a building, would be a double edge diffraction of a thick screen with the total travel distance $\tau = \tau_S + \tau_M + \tau_R$ and the distance $l = R_1 + R_2 + R_3$. Here, τ_M and R_2 are, respectively, the added time and distance for the sound to travel between the edges T_1 and T_2. The method assumes the top of the thick screen to be hard, setting the impedance $Z = \infty$.

$$\hat{p}(f) = \frac{1}{2}\hat{D}_1(f)\hat{D}_2(f)\frac{e^{j\omega\tau}}{l} \tag{2.29}$$

Choosing parameters for eq. 2.29 depend on the geometry of the wedge of which will not be explained further. For a double edge diffraction configuration, which is prominent in a wide barrier or two wedges, single diffraction coefficients are summed to make a double edge diffraction coefficient. When implementing a multiple diffraction configuration, as the number of diffraction edges increases, so do the necessary calculations. It is the main reason for the time increase when processing a complicated terrain.

Fresnel zones

A method that is known for computing the propagation and the strength of waves - let it be acoustic or radio waves propagating between a source and a receiver - is the Fresnel Zone method. The Fresnel Zone is an elliptical shaped body around the direct line of sight path between the source and the receiver as illustrated in figure 2.9. The image source method determines the path, but any obstacle within this volume can attenuate the waves along the transition path even if there is a direct line of sight.

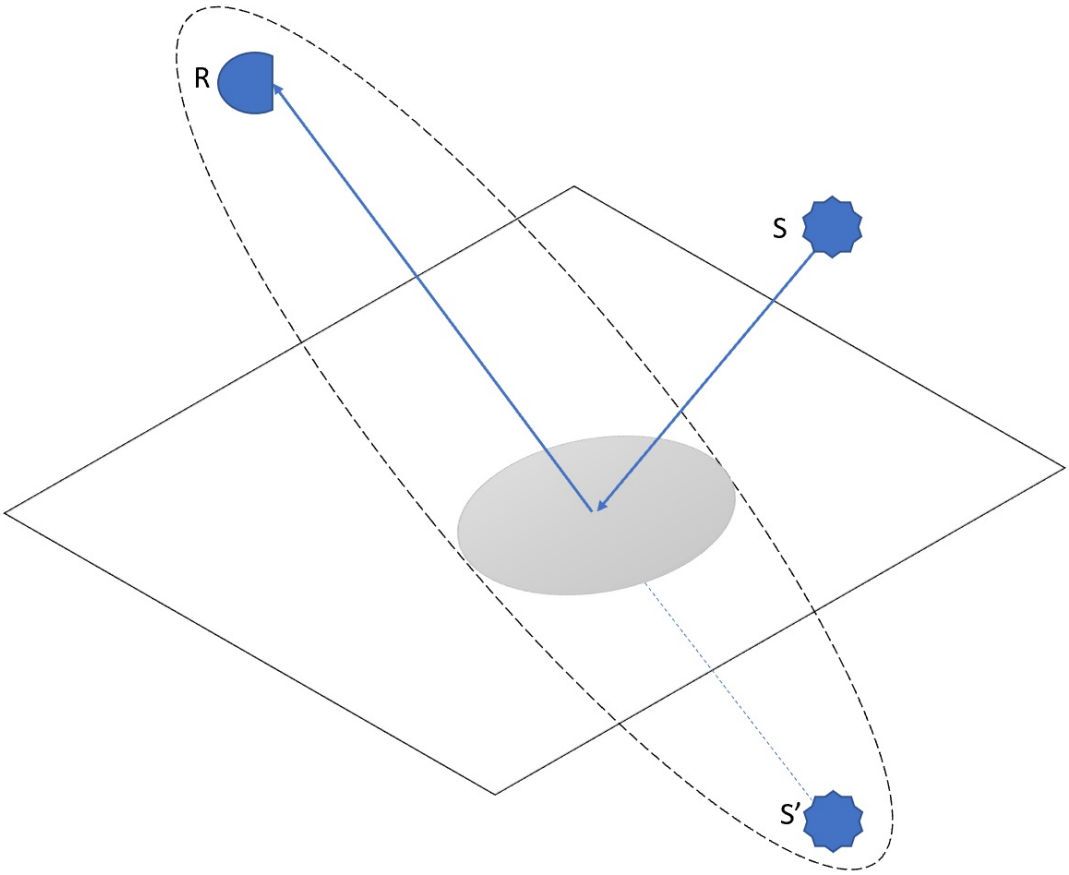

Figure 2.9: Fresnel zone between source and receiver.

2.8 Computing the Sound Pressure Level

According to to [6], the final expression of the SPL at the receiver depends on different Sub-Models. Some Sub-Models are not that relevant and will be regarded as not relevant for this thesis. One Sub-Model that are relevant will be mentioned to explain the main principle of how NORD2000 predicts the interaction between the propagating wave and ground to make reflections that attenuate the direct wave.

2.8.1 Single Screen With One Edge

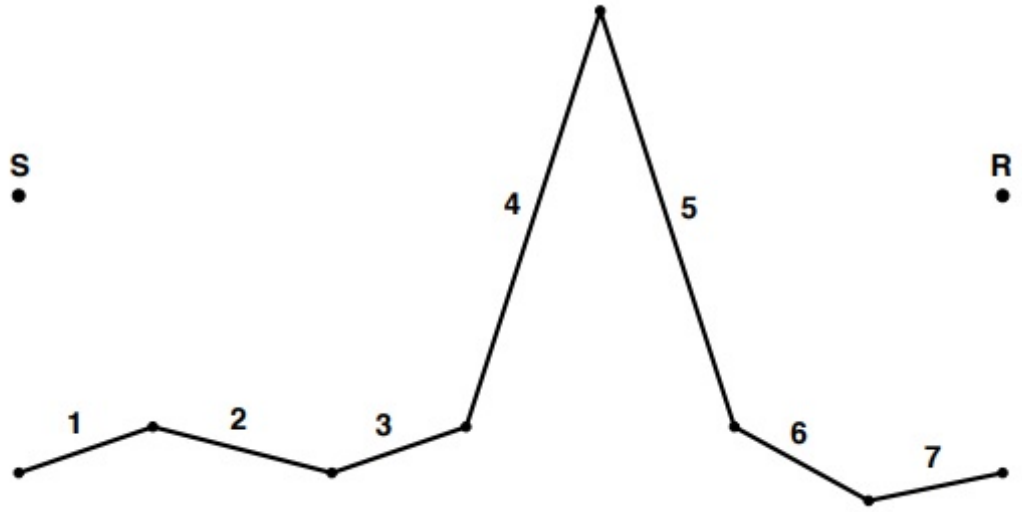

Figure 2.10: NORD2000 prediction of an uneven ground and a screen illustrated as a wedge [6].

This section is based on sub-model 4 in [6] and illustrated in figure 2.10. Assuming that the terrain profile has been found so that the number of reflecting segments is known. The total number of segments N_{ts} in the terrain profile used to label the following point numbers in the terrain profile:

- iSCR,1: Terrain point number closest to the source.
- iSCR,2: Terrain point number closest to the receiver.
- iSCR,T: Terrain point number closest to the diffracting edge.

The line segment representing the wedge closest to the source has the end coordinates $W_1 = (x_{iSCR,1}, z_{iSCR,1})$ and $T_1 = (x_{iSCR,T}, z_{iSCR,T})$. The line segment that represents the wedge face closest to the receiver has end coordinates $W_2 = (x_{iSCR,2}, z_{iSCR,2})$ and $T_1 = (x_{iSCR,T}, z_{iSCR,T})$. This can be shown in figure 2.10 where $iSCR, 1 = 4$, $iSCR, 2 = 6$ and $iSCR, T = 5$. The amount of reflecting line segments beneath the source and before the screen, are numbered $[N_{S1}\ N_{S2}] = [1\ (iSCR, 1 - 1)]$. The amount of reflecting line segments beneath the receiver and after the screen are numbered $[N_{R1}\ N_{R2}] = [iSCR, 2\ N_{ts}]$. This will be used in a simplified model called the base model to compute the different sound pressure levels and the wave reflection coefficients necessary. The base model illustrated in figure 2.11 shows the wedge defined by the points W_1, T_1 and W_2, the reflecting surfaces $P_{S1}P_{S2}$ and $P_{R1}P_{R2}$, and S_i R_i are the image sources to the source S and the receiver R respectively.

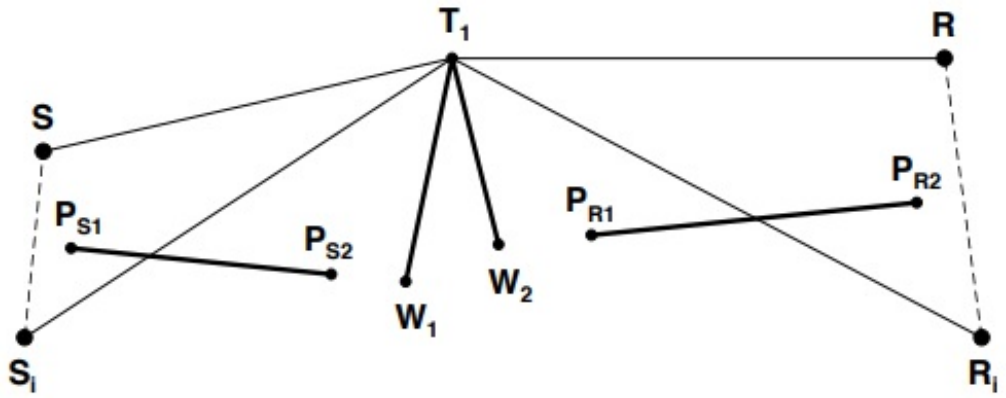

Figure 2.11: Geometry for the base model [6].

The straight line rays correspond to a non-refracting atmosphere that is comparable to a near-field configuration where meteorological factors are negligible. The image-source method is used to find the complex value of the pressure at the receiver $\hat{p}$.

$$\hat{p} = \hat{p}_1 + \hat{Q}_1\hat{p}_2 + \hat{Q}_2\hat{p}_3 + \hat{Q}_1\hat{Q}_2\hat{p}_4 \tag{2.30}$$

Here, $\hat{p}$ is expressed with the diffracted sound pressure from the source to the receiver which is denoted $\hat{p}_1$, the diffracted sound pressure from the image source to the receiver $\hat{p}_2$, the diffracted sound pressure from the source to the image receiver $\hat{p}_3$ and $\hat{p}_4$ which is the diffracted sound pressure from the image source to the image receiver. Also, $\hat{Q}_1$ and $\hat{Q}_2$ are, respectively, the denotations of the spherical wave reflection coefficients from the source and receiver side of the screen. The spherical wave reflection coefficients is a function of frequency f along travel time τ along the reflected ray and the ground impedance $Z_G(f_m)$ [6]. All values are complex values.

Before applying the Fresnel-zone interpolation, the propagation effect must be obtained by using the sound pressure relative to the free-field sound pressure denoted p_0 and separating the screen effect and the ground effect as shown in eq. 2.31.

$$\frac{\hat{p}}{\hat{p}_0} = \frac{p_{1,ff}}{p}_0\left(1 + \hat{Q}_1\frac{\hat{p}_2}{\hat{p}_1} + \hat{Q}_2\frac{\hat{p}_3}{\hat{p}_1} + \hat{Q}_1\hat{Q}_2\frac{\hat{p}_4}{\hat{p}_1}\right) \tag{2.31}$$

Here $\hat{p}_{1,ff}$ is the diffracted sound pressure from source to receiver
in a free field that has a different sound speed profile from $\hat{p}_1$. $\hat{Q}_1$ and $\hat{Q}_2$
are modified at the base model for increased efficiency. These modified reflection coefficients are multiplied by a real number w which is determined by Fresnel-zones so the modified coefficients yields $\hat{Q'}_1 = w_{Q_1}\hat{Q}_1$ and$\hat{Q}'_2 = w_{Q_2}\hat{Q}_2$. These are inserted to eq. 2.31:

$$\frac{\hat{p}}{\hat{p}_0} = \frac{\hat{p}_{1,ff}}{\hat{p}_0}\left(1 + \hat{Q'}_1\frac{\hat{p}_2}{\hat{p}_1} + \hat{Q'}_2\frac{\hat{p}_3}{\hat{p}_1} + \hat{Q'}_1\hat{Q'}_2\frac{\hat{p}_4}{\hat{p}_1}\right) = \hat{p}_{SCR}\hat{p}_G \tag{2.32}$$

where the effect from the screen $\hat{p}_{SCR}$ is expressed as follows:

$$\hat{p}_{SCR} = \frac{\hat{p}_{1,ff}}{\hat{p}_0} \tag{2.33}$$

and the effect from the ground $\hat{p}_G$:

$$\hat{p}_G = \left(1 + \hat{Q}'_1 \frac{\hat{p}_2}{\hat{p}_1} + \hat{Q}'_2 \frac{\hat{p}_3}{\hat{p}_1} + \hat{Q}'_1 \hat{Q}'_2 \frac{\hat{p}_4}{\hat{p}_1} = \hat{p}_{SCR} \hat{p}_G\right) \tag{2.34}$$

The screen effect $|p_{SCR}|$ and the ground effect $|p_G|$ are computed where the ground effect will be found for each terrain segment, so $|p_{G,i1,i2}|$ is denoted segment $i1$ on the source side and $i2$ on the receiver side. The Freznel-Zone weights $w''_{i1}(f)$ and $w''_{i2}(f)$ are normalized by the formulas in [6] and the final weights of the spherical-wave reflections w_{Q_1} and w_{Q_2} are found.

$$\Delta L_t = 20 \log_{10} \left(|\hat{p}_{SCR}(f)| \prod_{i1=N_{S1}}^{N_{R1}} \prod_{i2=N_{R1}}^{N_{R2}} |\hat{p}_{G,i1,i2}|^{w'_{i1}(f) w'_{i2}(f)} \right) \tag{2.35}$$

2.8.2 Single Screen With Double Edges

The other Sub-Model looks at the contribution of terrain with one screen having two edges of which computes the SPL the same way as eq. 2.35, but instead using eq. 2.29 and some geometrical considerations from [6]. This is quite complicated and will not be elaborated further.

Chapter 3

Methodology

The scope of this thesis is to compare different prediction methods and how well they predict the effects of diffraction in a realistic environment. Outdoor measurements with a single edge and a double edge configuration are needed as suitable references. This section will explain in detail the measurements that were conducted, and the computer simulations made in SoundPlan 8.0. An outdoor measurement where the goal is to study diffraction is not easy to implement. The specific areas have to meet specific requirements. Firstly, there has to be a low background noise level so that the measurements could be conducted using a controlled noise source. Secondly, the source and receiver should be placed in an open area to avoid any substantial disturbances from side reflections.

A wooden screen at a bus-station parking lot called Bekkestua located in Bærum Norway was chosen as the optimal place for conducting single diffraction measurements. Most screens are built along roads, which makes it challenging to do repeatable measurements with a controlled noise source, which was the main reason why Bekkestua was chosen since it was several hundred meters from any traffic. Also, the screen was put up between the parking lot and a small football field in a quiet neighbourhood, so it was made sure that no significant noise sources were affecting the measurements.

Finding a building to study double diffraction in favourable conditions was a bit more complicated. Monolitten kindergarten was chosen for its uniquely rectangular shape and its distance from other buildings. The kindergarten was located next to a road so that some traffic could attenuate the measurements. The building itself was a construction made of several container barracks placed in a two by sixteen formation and stacked with two containers on top so that the building had two floors. The containers are made of steel. The flat roof was one of the main reasons for choosing this building because it eliminates any effect on the unwanted diffractions that a pitched roof might have.

The topography at each location was measured using a laser and tape measurer and are presented in figure 3.2, 3.3, 3.5 and 3.6. The measured geometrical properties were collected and implemented in SoundPlan 8.0 to make measured and simulated results more comparable. All post-processing and figures were made using Matlab R2017a.

3.1 Field Measurements

The noise source was a Qsources Qohm omnidirectional speaker, which has a frequency range at 1/3 octaves from 50 Hz to 16 kHz [13]. The speaker was placed on a stand, connected to a Nor-280 power amplifier[14] and as close to the ground as possible. The source was emitting

punk noise and the microphones were placed at each receiver position indicated in figures 3.2, 3.3, 3.5 and 3.6. Two were calibrated and placed at two different measurement heights, 2 meters (channel 1) and 5 meters (channel 2) from the ground. The microphone in channel 1 was a NOR-1220 microphone [15] with a NOR-1201 pre-amplifier [16]. The microphone in channel 2 was a NOR-1225 microphone [17] with a NOR-1209 pre-amplifier [18]. The microphones were set in a dual-channel configuration using the Norsonic nor150 sound and vibration analyser. The data were sampled at a rate of 12 kHz, measured at a time frame of 15 seconds and stored as 1/3 octave bands levels. Mainly to meet the criteria of the NORD2000 method, but it also gave higher precision, which means that the sound was measured simultaneously at two different heights at one receiver position. The measurements were then repeated for the other receiver positions. After all of the receiver positions were measured, a noise mapping of the source was conducted as described in section 3.1.4. Since the calculated results were retrieved in the 1/1-octave band, the results were converted from 1/3-octave to the same band to be comparable.

3.1.1 Single Screen, Bekkestua Buss Lot

(a) Bus parking lot. (b) Football field.

Figure 3.1: Pictures of both sides of the screen at Bekkestua.

Bekkestua had some bus activity on the day when the measurements were conducted, but the measurement was conducted so that no significantly disturbing activity was present. There had also been an arrangement to remove all busses in the proximity of the area to meet the requirement of open space around the sound source (figure 3.1a). However, there was some sparsely filled vegetation, as seen in figure 3.1b, in the direct propagation path that could be a source of error.

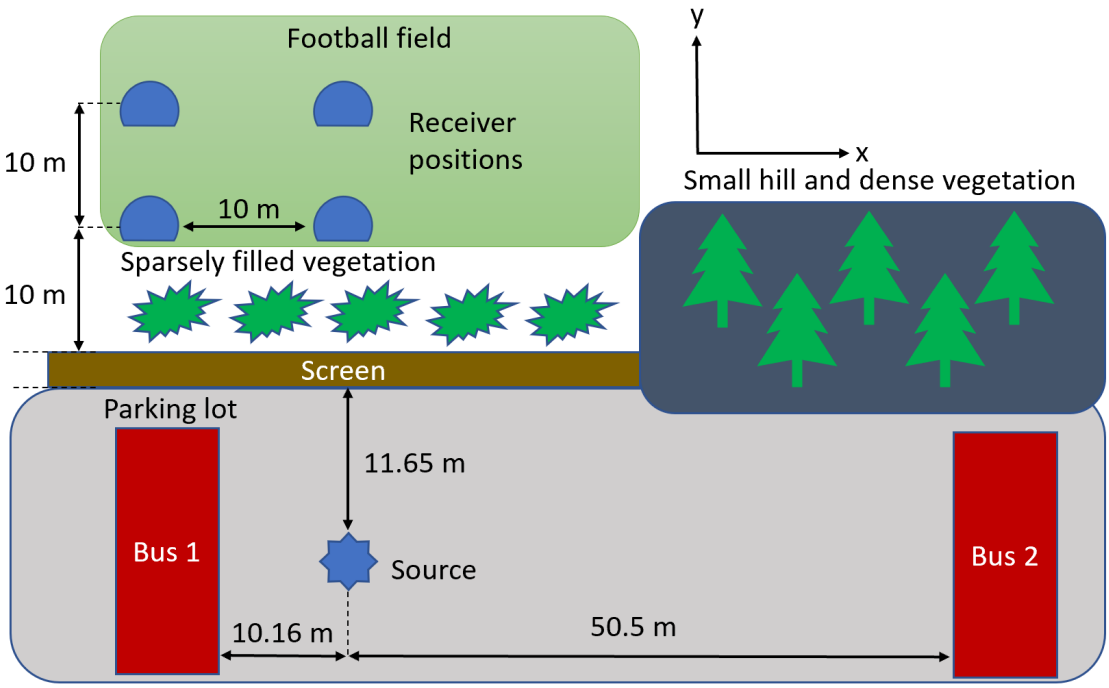

Figure 3.2: 2D surface illustration of Bekkestua.

The illustration in figure 3.2 shows an overview of the area surrounding the screen. The receiver positions were chosen so that the equivalent sound pressure levels $L_{A,eq}$, could be mapped across the football field. The microphone positions were chosen to be 10 meters and 20 meters from the screen in the direct line of the source. There was also measurements conducted 10 meters perpendicular from the direct line and with same parallel distance from the screen. At each position, two measurements were conducted to ensure consistency.

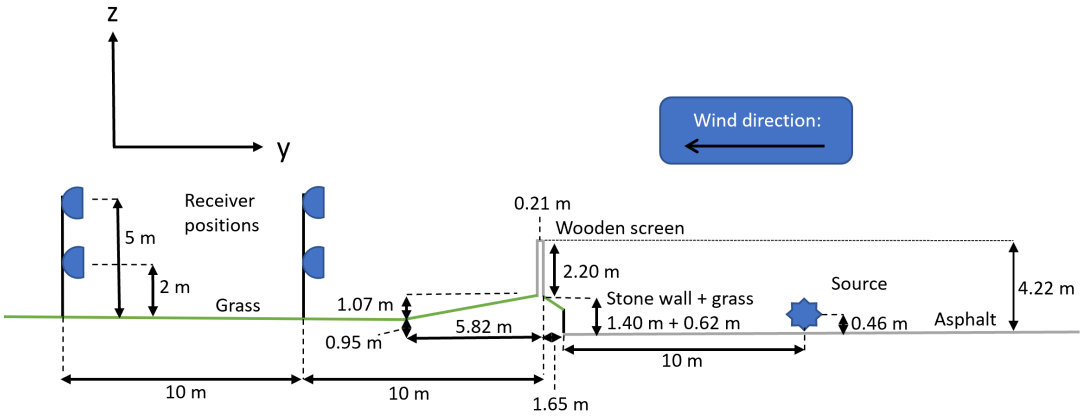

Figure 3.3: Side view of Bekkestua showing the geometrical properties.

Figure 3.3 shows that the screen is standing on a stone wall with a small grass hill on top

with a combined height of 4.22 meters.

Weather conditions

As indicated in figure 3.3, the wind had optimal conditions since the direction was the same as the sound propagation that was measured. Also, at 5 meters measurements, the maximum wind velocity was 2 m/s. At 2 meters the microphone was shielded from wind exposure by the screen, so at this height, the wind speed was assumed to be close to 0 m/s. The wind speed was not physically measured but retrieved from reliable weather forecasts at the time the measurements were conducted.

3.1.2 Building, Monolitten Kindergarten

(a) Monolitten at the source side. (b) Monolitten at the receiver side.

Figure 3.4: Monolitten at the front and back respectively.

Monolitten kindergarten had a parking lot at the front entrance with a playground at the back. The playground had some artefact such as a swing and a sandpit, but they were so far away from the measurement positions that their impact was considered to be negligible. There was a keen interest in observing the diffraction close to the wall, so including the same measurement setup as Bekkestua, two positions close to the wall at 2 m were measured adding up a total of six measurement points with two different measurement heights. Also, a background sound pressure measurement at each position was conducted, which will be elaborated in section 3.1.3.

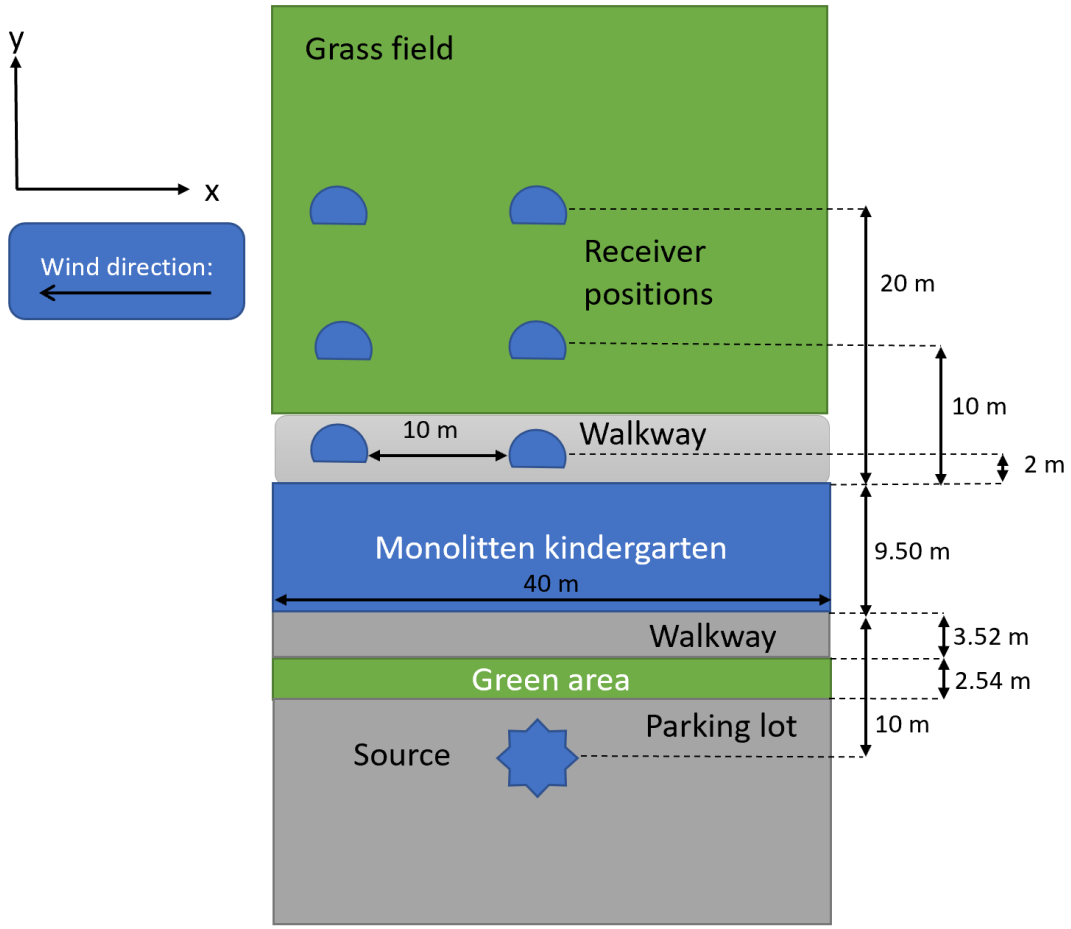

Figure 3.5: 2D overview of the area surrounding Monolitten kindergarten.

The illustration in figure 3.5 shows an overview of the area surrounding the building. The receiver positions were chosen so that the equivalent sound pressure levels $L_{A,eq}$, could be mapped across the playground. There was a single container at the left end of the building which could give rise to some side reflections, but those were assumed negligible.

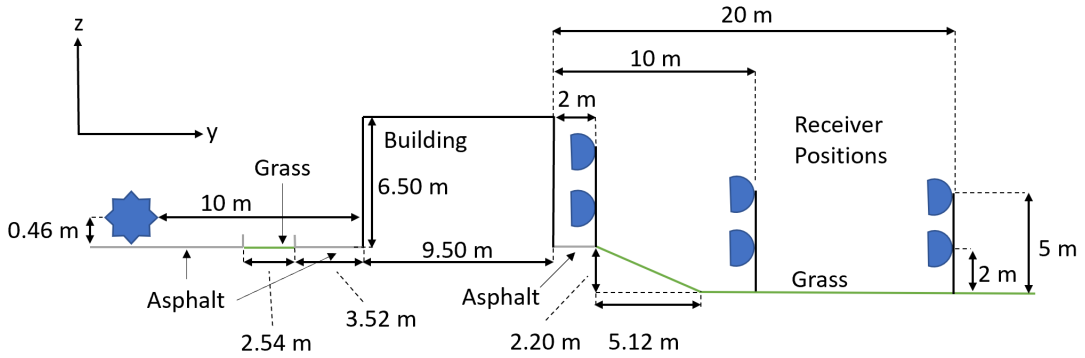

Figure 3.6: Side view illustration of the building showing the geometrical properties.

As observed in figure 3.6, the building is standing on top of a small hill overseeing the grass field, which is the playground. A small strip of asphalt is present before the grassy slope leading down to the playground. Monolitten is levelled with the parking lot, and a small strip of grass is present between the source and the building.

Weather conditions

The wind was slightly more challenging at Monolitten than at Bekkestua. As shown in figure 3.5, the area was exposed to side wind, although the influence from the wind was experienced to be negligible. The wind was assumed to have the same velocity (1.7 m/s) at both measurement heights, but these data were also retrieved from the weather forecast and not measured directly.

3.1.3 Possible Sources of Error

Single Screen

The screen at Bekkestua was quite old and had clear signs of degeneration. As figure 3.7 shows, there are a few parts of the screen that have significant cracks which could be a clear source of error, and some sound leakages must be considered when discussing the results.

Figure 3.7: Wooden screen at Bekkestua, showing signs of decay and some leakages.

One of the buses on the left side of the source was supposed to be moved, but due to some technical difficulties with the bus, this could not be completed. The possibility to move the source further to the right was evaluated, but since there were dense vegetation and a hill on the left-hand side that could have a more significant negative impact on the measurements, it was decided to follow through with the initial setup. Even though the distance between the bus and the source was approximately 10 meters, there might be some side reflections interfering with the direct noise.

Building

As seen in figure 3.6, the receiver positions at two meters from the wall are higher than the others, due to uneven topography which led to some differences between the equivalent sound level, assuming different effect from diffraction and not only by distance.

During measurements, there were still cars in the parking lot, and some of them were close to the source which can be a problem since some near field reflections might affect the direct emission from the source. A picture showing the parking lot is presented in figure 3.8a.

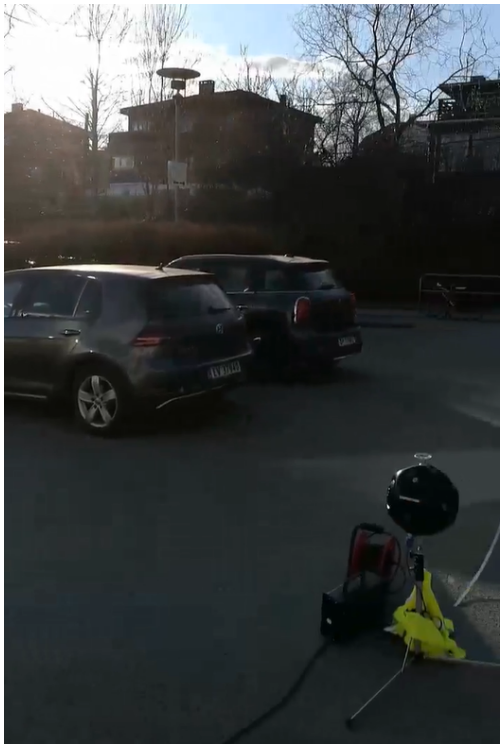

(a) Parking lot.

(b) Air condition system.

Figure 3.8: Possible sources of error at Monolitten.

On the receiver side, there was some substantial noise pollution caused by an air conditioning system (figure 3.8b) placed close to the first receiver position in direct line of the source. The air conditioner noise level was reduced until a minimum just before the first measurement, but it was still noticeable to a small extent. Because of this potential source of error, it was decided to do background measurements at all positions to ensure that there was no significant interference with the measured results.

3.1.4 Calibration of the Source

One of the questions that were addressed is how one can remake the speaker in the simulation so that the measurement and the simulated results are comparable. So, the following method was found to be the best solution. The equivalent SPL of the speakers was measured at close range at two different distances and two heights. By measuring the equivalent SPL of the simulated speaker at the same positions, it was possible to alter the speaker so that the measured output matched with the real measurements. The measurement setup is illustrated in figure 3.9 and in figure 3.10.

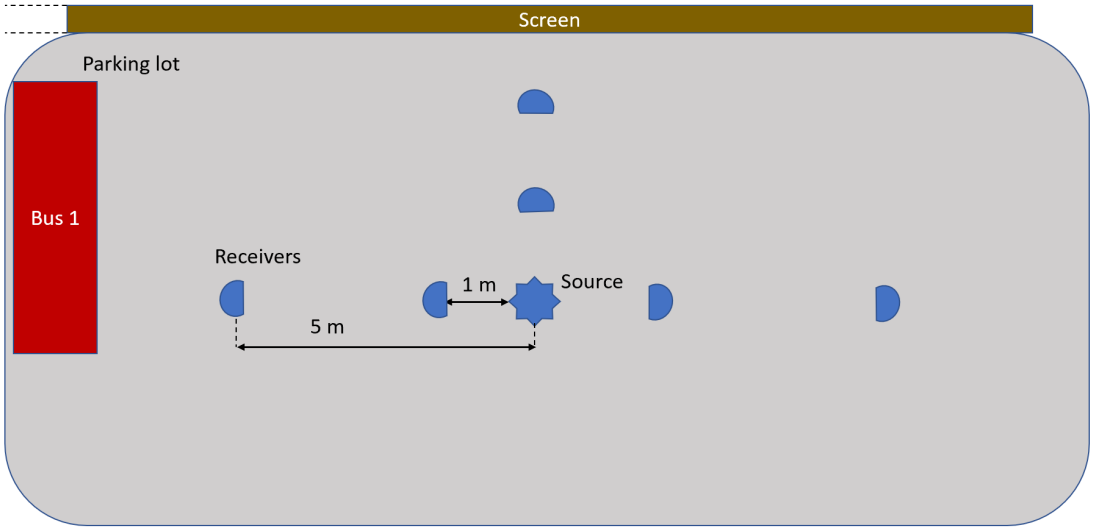

Figure 3.9: Measurement setup for speaker calibration at Bekkestua.

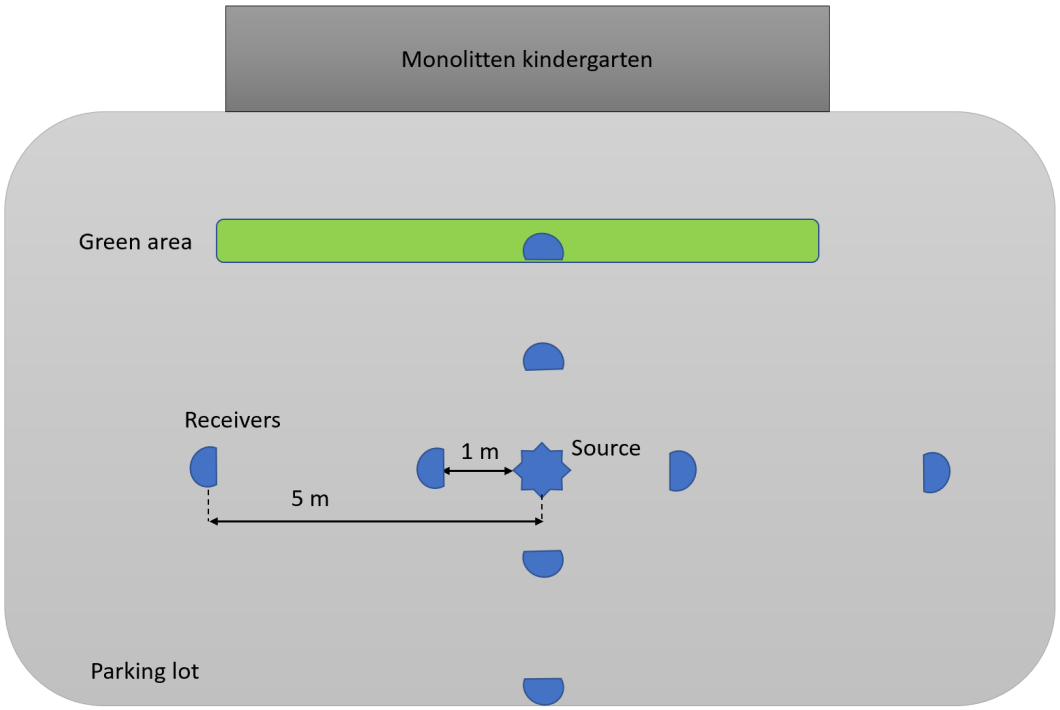

Figure 3.10: Measurement setup for speaker calibration at Monolitten.

It was chosen to have measurements in the near field at 1 meter and 5 meters in the front, to the left and right of the speaker, giving it a total amount of 6 calibration positions. The difference between the speaker at Bekkestua and Monolitten is that at the building, it was chosen to do

additional measurements at the back of the speaker. A total of 8 calibration positions were made to see if the cars at the parking lot had any effect on the source emission. The setup with the numbering of positions is presented in figure 3.11.

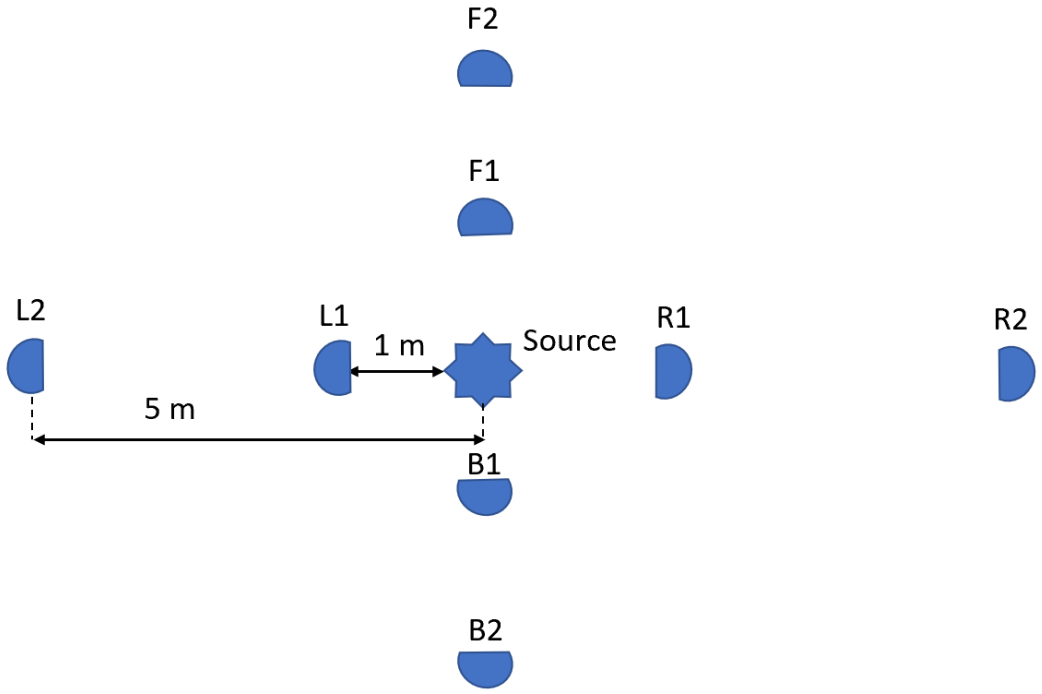

Figure 3.11: Position of receivers at the front (F), right (R), left (L) and back (B).

These measurements were conducted at the heights of 2 meters and 3.8 meters. Unfortunately, the measurements at the building parking lot at 2 meters were corrupted, probably due to some problem with the connection. So, only the measurements at a height of 3.8 meters were collected. The data of the equivalent SPL are presented in chapter 4.

Calculations of a correction factor

In post-processing, it was found in the speaker does not emit pink noise with the same level at all octave bands [13] which is typical for most speakers; thus, a correction factor was implemented. The measured SPL at a 1-meter distance and 3.8-meter height were log-summed, and the mean was taken at each octave band as shown in Eq. 3.1[1]. The log-sum (eq. 3.2) was assumed to be the closest representation of the real pink-noise level. In eq. 3.1 i is the amount of octave bands.

$$\Delta_{speaker} = \sum_{i=1}^{8} 10 \log_{10} \left(\frac{10^{L_{L1,i}/10} + 10^{L_{F1,i}/10} + 10^{L_{R1,i}/10}}{3} \right) \tag{3.1}$$

[1]For the building, the calibration point in the back of the speaker was added as well, dividing it by four positions instead of three.

$$L_{speaker,pink} = 10\log_{10}\left(\frac{10^{\frac{\Delta_{speaker,63}}{10}} + 10^{\frac{\Delta_{speaker,125}}{10}} + ... + 10^{\frac{\Delta_{speaker,8000}}{10}}}{8}\right) \tag{3.2}$$

Finally, the correction factor was computed as follows:

$$\Delta_{corr} = \Delta_{speaker} - L_{speaker,pink} \tag{3.3}$$

The correction factor was then subtracted from the measured results.

3.2 SoundPlan Simulations

The SoundPlan simulations were conducted by implementing the geometrical properties retrieved from the physical measurements illustrated in figures 3.2, 3.3, 3.5 and 3.6. Three simulations were run in the same model, and the only tuning was the speaker SWL L_W so that they would be comparable the real speaker. The speakers at the single screen simulation and the building simulation had a L_W of 112.2 dB and 112.4 dB respectively. Table 3.1 shows parameters that were chosen for the asphalt and grass areas.

Method	**NORD96**	**CNOSSOS-EU**	**NORD2000**
Asphalt	G = 0 (Hard Surface)	G = 0 (Type G)	$\sigma = 20000$ (Type G)
Grass	G = 1 (Porous surface)	G = 1 (Type C)	$\sigma = 80$ (Type C)

Table 3.1: Parameters chosen for determining ground attenuation from appendix B.

For Nord2000, the ground roughness was set to class N meaning that the roughness $\sigma_r = 0$ as shown in appendix B.4.

3.2.1 Single Screen

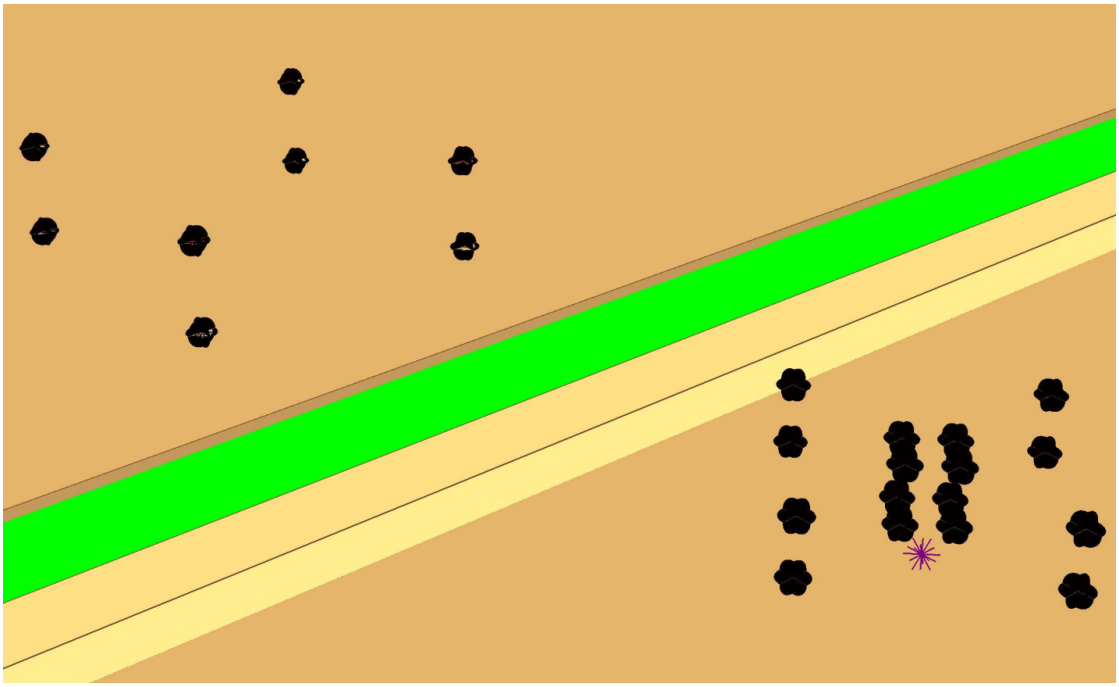

Figure 3.12: Screenshot of SoundPlan model of Bekkestua.

Figure 3.12 shows a 3D view of the model in SoundPlan. The black dots represent the measurement points, the red point represent the source, and the screen is marked in green.

The brick wall had the same ground factor as the asphalt, and the screen had an absorption coefficient $\alpha = 0.206$, meaning a reflection loss of 1 dB. α was chosen on the fact that the real screen was a wooden screen.

3.2.2 Building

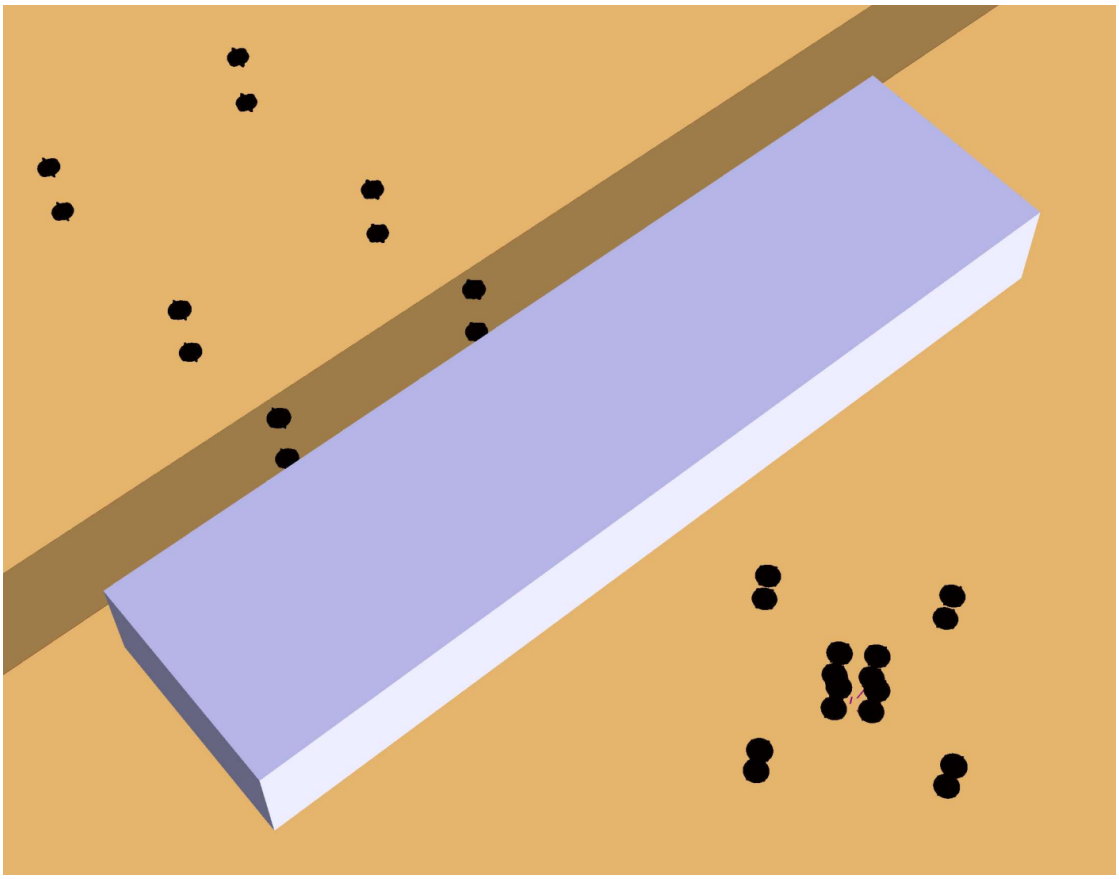

Figure 3.13: Screenshot of SoundPlan model of Monolitten.

Figure 3.13 shows a 3D view of the model in SoundPlan. The black dots represent the measurement points, the red point represent the source, and the building is the grey, box-shaped object. Since the building was a structure made of steel, an absorption coefficient was chosen to be $\alpha = 0$ which give a reflection loss of 0 dB.

Chapter 4

Results

4.1 Speaker Calibration

Table 4.1 presents the measured calibration positions around the speaker. The sections marked "-" were not collected and "X" are collected data that were corrupted.

Table 4.3, 4.4, 4.5, 4.6, 4.7, and 4.8 shows the measured equivalent SPL at each location comparing prediction methods individually with the measured values.

	Bekkestua		**Monolitten**	
Position	$L_{A,eq}$ at 2 m	$L_{A,eq}$ at 3.8 m	$L_{A,eq}$ at 2 m	$L_{A,eq}$ at 3.8 m
F1	99.0	93.5	X	93.7
F2	90.9	89.4	X	89.7
R1	98.8	93.3	X	93.6
R2	90.2	90.2	X	89.9
L1	98.9	93.3	X	94.1
L2	90.7	90.1	X	89.8
B1	-	-	X	94.1
B2	-	-	X	89.7

Table 4.1: $L_{A,eq}$ [dBA] measured at certain positions surrounding the speaker.

Δ_{corr} **at Bekkestua and Monolitten**								
Octave band [Hz]	63	125	250	500	1000	2000	4000	8000
Bekkestua [dBA]	-9.3	-8.5	4.3	3.9	2.7	-2.6	-6.9	-20.0
Monolitten [dBA]	-10.3	-7.9	4.5	4.2	3.3	-2.0	-6.6	-18.4

Table 4.2: Correction factor for pink noise using eq. 3.3.

Figure 4.1 and 4.2 presents the speaker calibration with and without the correction from table 4.2 marked *Corr* (Corrected) and *Uncorr* (Uncorrected) respectively. Also, NORD96, CNOSSOS-EU and NORD2000 are labeled *N96*,*CNO* and *N2000*, respectively.

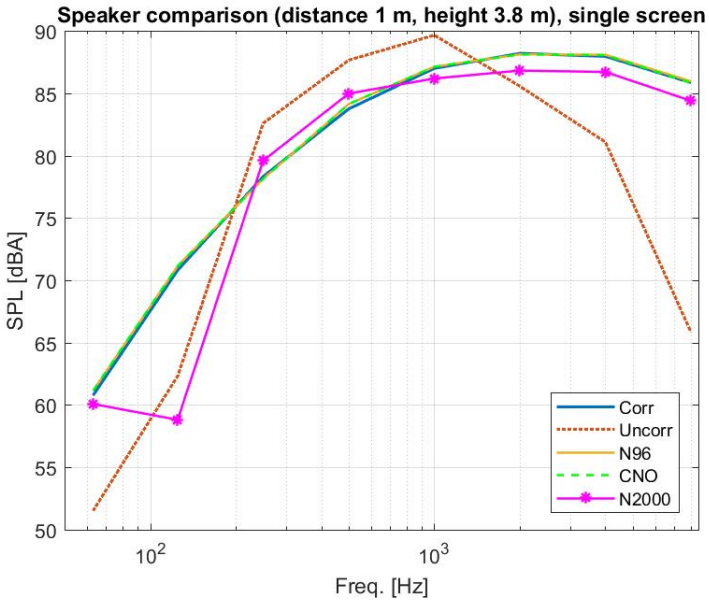

Figure 4.1: Comparison of speaker SPL from the single screen.

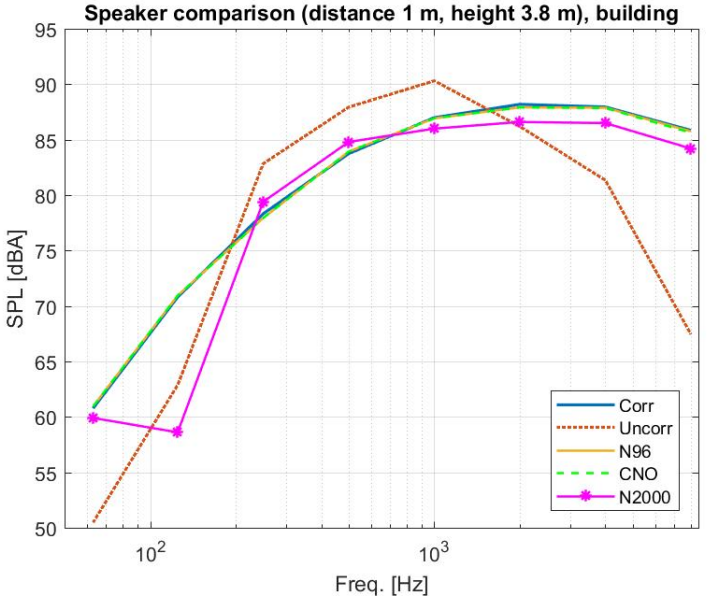

Figure 4.2: Comparison of speaker SPL from the building.

4.1.1 Single Screen

	$L_{A,eq}$ **[dBA] at 2 m**			$L_{A,eq}$ **[dBA] at 3.8 m**		
Position	Measured	Simulated	Difference	Measured	Simulated	Difference
F1	99.0	100.0	-1	93.5	94.0	-0.5
F2	90.9	90.0	0.9	89.4	88.9	0.5
R1	98.8	100.0	-1.2	93.3	94.02	-0.7
R2	90.2	90.0	0.2	90.2	89.0	1.3
L1	98.9	100	-1.0	93.3	94.0	-0.7
L2	90.7	90.0	0.7	90.1	88.9	1.2

Table 4.3: Single Screen, NORD96.

	$L_{A,eq}$ **[dBA] at 2 m**			$L_{A,eq}$ **[dBA] at 3.8 m**		
Position	Measured	Simulated	Difference	Measured	Simulated	Difference
F1	99.0	97.9	1.1	93.5	92.9	0.6
F2	90.9	88.9	2.0	89.4	87.6	1.8
R1	98.8	97.9	0.9	93.3	92.9	0.4
R2	90.2	88.9	1.3	90.2	87.6	2.6
L1	98.9	97.9	1.0	93.3	92.9	0.4
L2	90.7	88.9	1.82	90.1	87.6	2.5

Table 4.4: Single Screen, CNOSSOS-EU.

	$L_{A,eq}$ **[dBA] at 2 m**			$L_{A,eq}$ **[dBA] at 3.8 m**		
Position	Measured	Simulated	Difference	Measured	Simulated	Difference
F1	99.0	99.8	-0.8	93.5	93.9	-0.4
F2	90.9	89.9	1.0	89.4	88.7	0.7
R1	98.8	99.8	-1	93.3	93.9	-0.6
R2	90.2	89.9	0.3	90.2	88.9	1.4
L1	98.9	99.8	-0.9	93.3	93.9	-0.6
L2	90.7	89.9	0.8	90.1	88.9	1.3

Table 4.5: Single Screen, NORD2000.

4.1.2 Building

	$L_{A,eq}$ **[dBA] at 3.8 m**		
Position	Measured	Simulated	Difference
F1	93.5	95.2	-1.7
F2	89.4	90.6	-1.2
R1	93.3	95.2	-1.9
R2	90.2	90.4	-0.2
L1	93.3	95.2	-1.9
L2	90.1	90.4	-0.3
B1	95.2	94.1	1.1
B2	90.3	89.7	0.6

Table 4.6: Building, NORD96.

	$L_{A,eq}$ **[dBA] at 3.8 m**		
Position	Measured	Simulated	Difference
F1	93.5	93.5	0.0
F2	89.4	88.0	1.4
R1	93.3	93.3	0.0
R2	90.2	87.7	2.5
L1	93.3	93.3	0.0
L2	90.1	87.7	2.4
B1	95.2	93.3	1.9
B2	90.3	87.6	2.7

Table 4.7: Building, CNOSSOS-EU.

	$L_{A,eq}$ **[dBA] at 3.8 m**		
Position	Measured	Simulated	Difference
F1	93.5	93.7	-0.2
F2	89.4	87.9	1.5
R1	93.3	93.7	-0.4
R2	90.2	88.8	1.4
L1	93.3	93.7	-0.4
L2	90.1	88.8	1.3
B1	95.2	93.7	1.6
B2	90.3	88.7	1.6

Table 4.8: Building, NORD2000.

4.2 Measurements

Figure 4.3 and 4.4 are references to the following figures where the positions are numbered for simplicity. The background noise at position 21 were mistakenly not conducted and are therefore not added to figure 4.18 and 4.22. The plotted background noise is labeled *Back*.

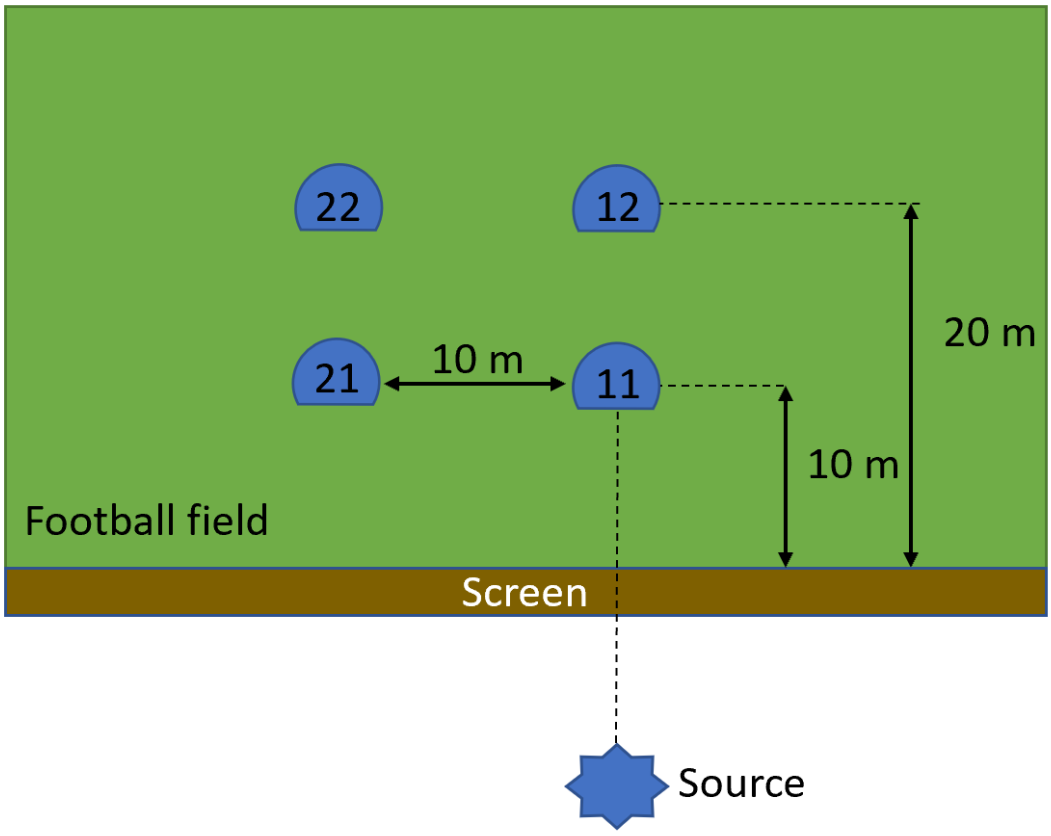

Figure 4.3: Setup numbering the receiver positions at Bekkestua.

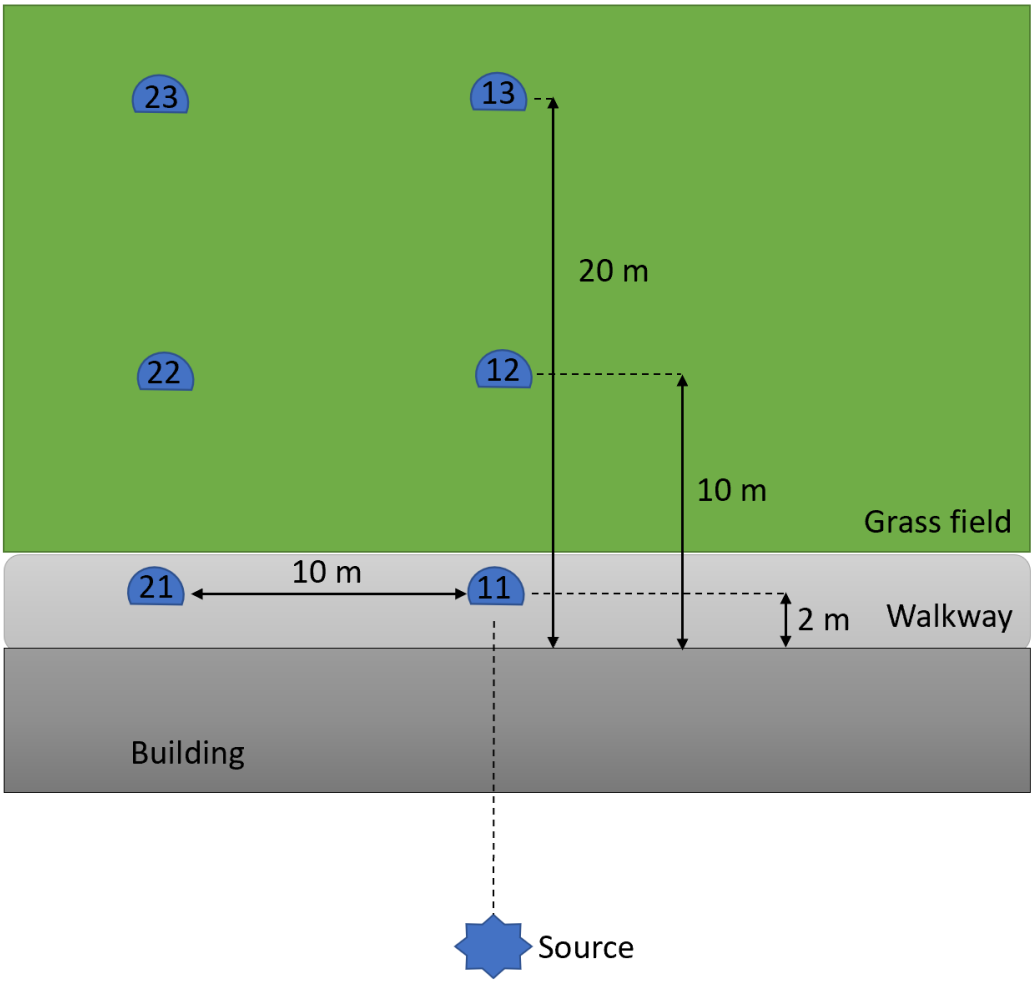

Figure 4.4: Setup numbering the receiver positions atMonolitten.

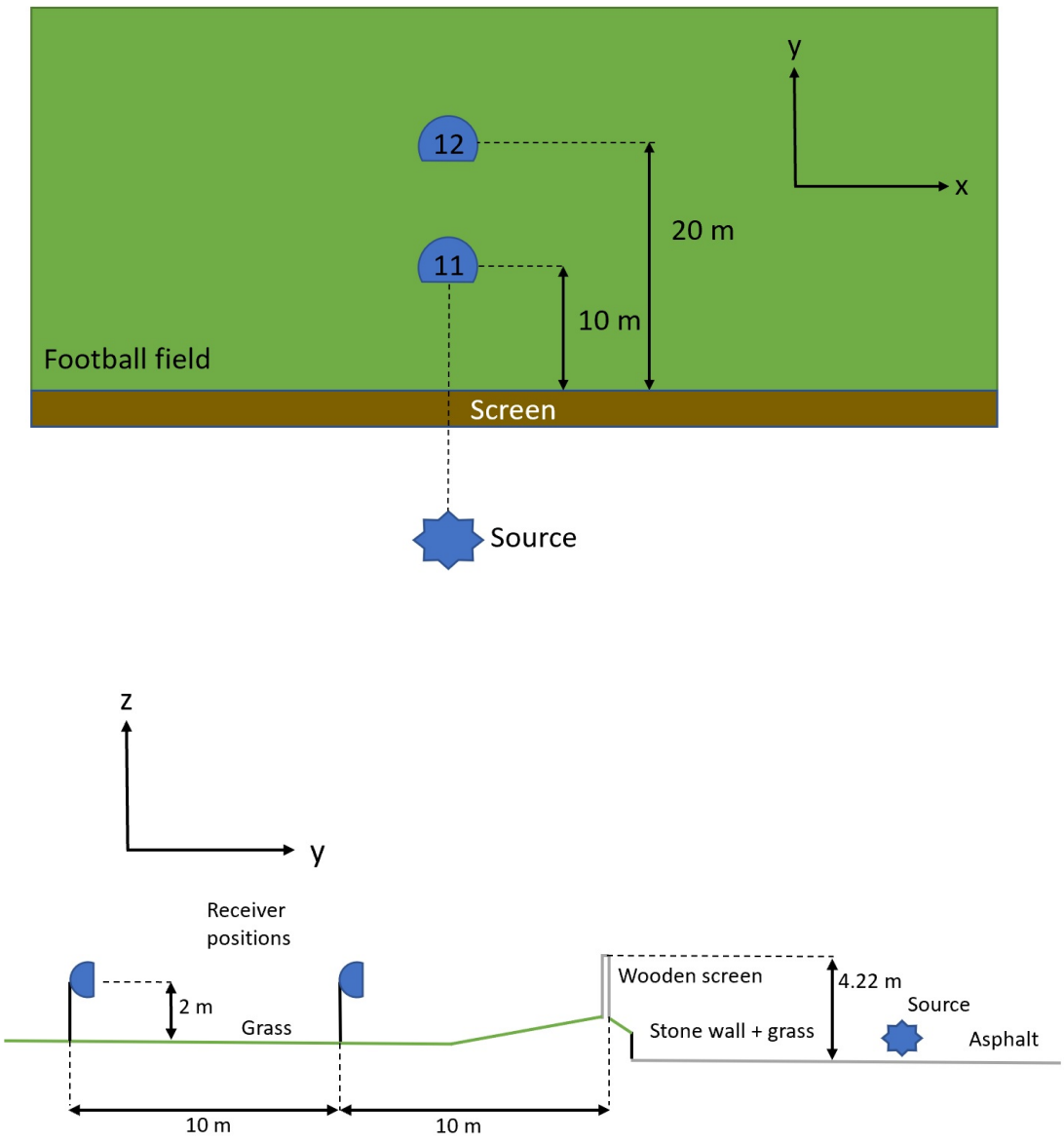

Figure 4.5: Setup highlighting position 11 and 12 at single-edge diffraction measurements with results presented in figure 4.6.

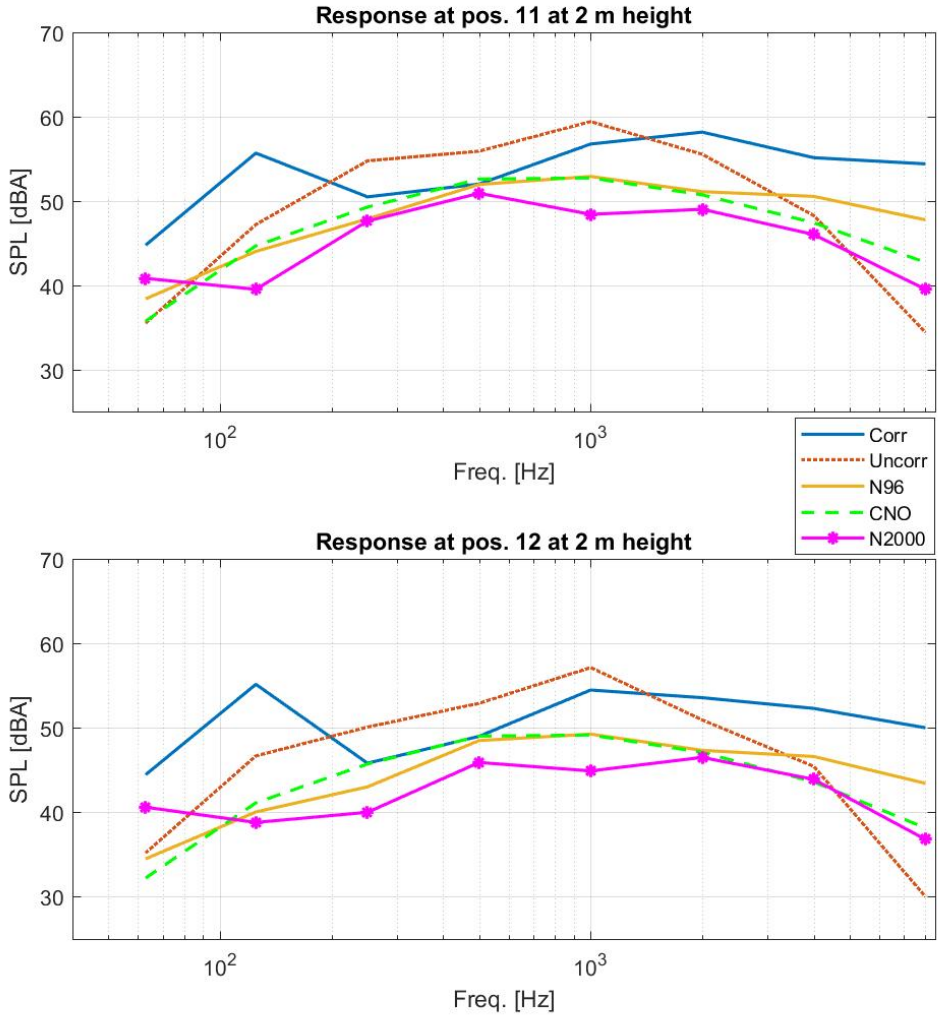

Figure 4.6: SPL of single-edge diffraction measurements showing the corrected speaker (*Corr*), the uncorrected speaker (*Uncorr*), NORD96 (*N96*), CNOSSOS-EU (*CNO*) and NORD2000 (*N2000*).

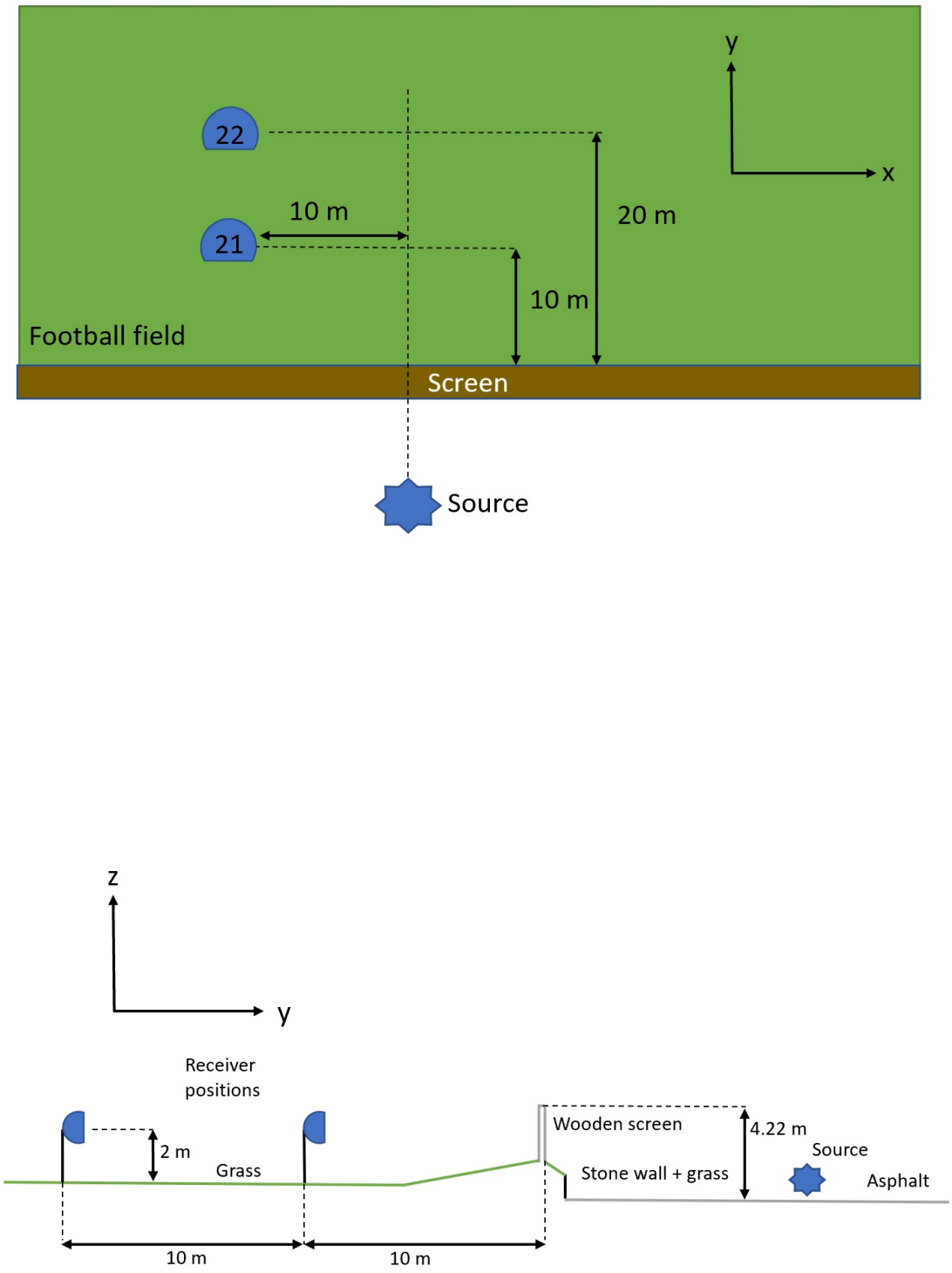

Figure 4.7: Setup highlighting position 21 and 22 at single-edge diffraction measurements with results presented in figure 4.8.

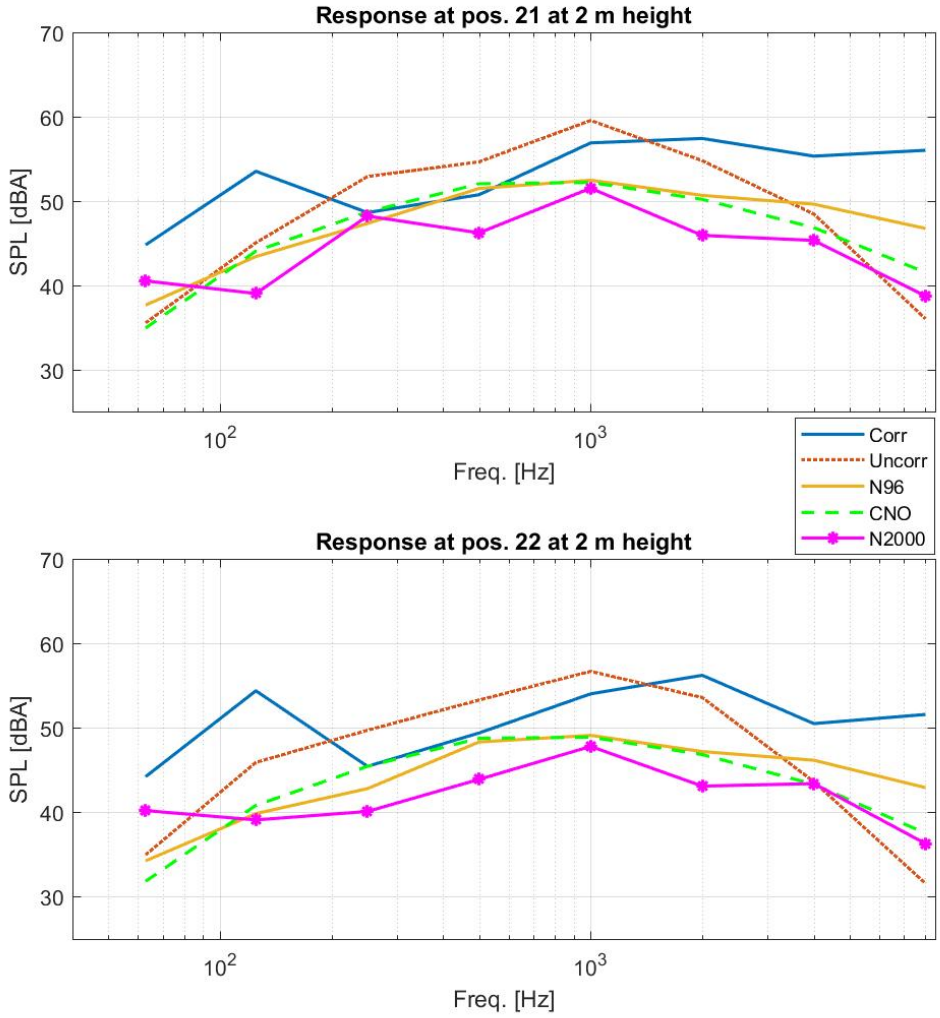

Figure 4.8: SPL of single-edge diffraction measurements showing the corrected speaker (*Corr*), the uncorrected speaker (*Uncorr*), NORD96 (*N96*), CNOSSOS-EU (*CNO*) and NORD2000 (*N2000*).

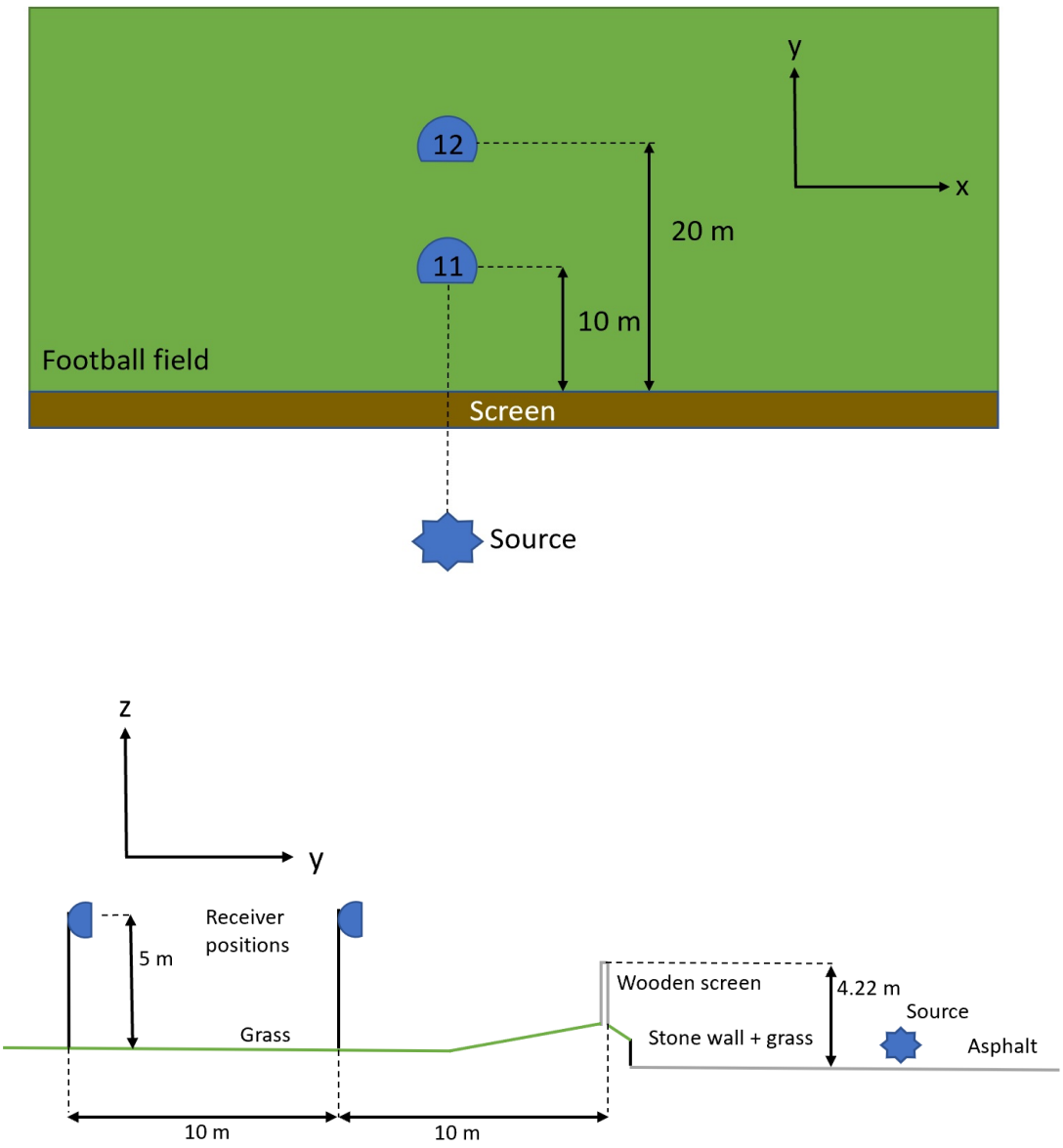

Figure 4.9: Setup highlighting position 11 and 12 at single-edge diffraction measurements with results presented in figure 4.10.

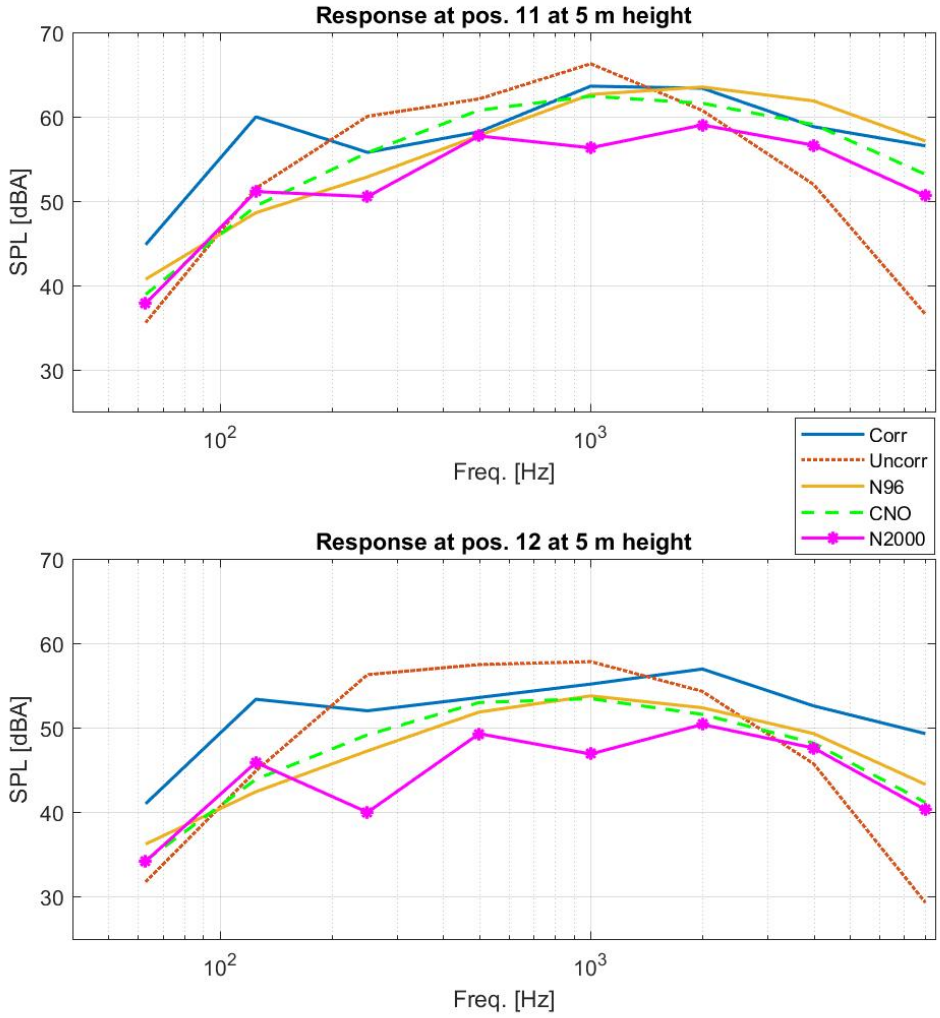

Figure 4.10: SPL of single-edge diffraction measurements showing the corrected speaker (*Corr*), the uncorrected speaker (*Uncorr*), NORD96 (*N96*), CNOSSOS-EU (*CNO*) and NORD2000 (*N2000*).

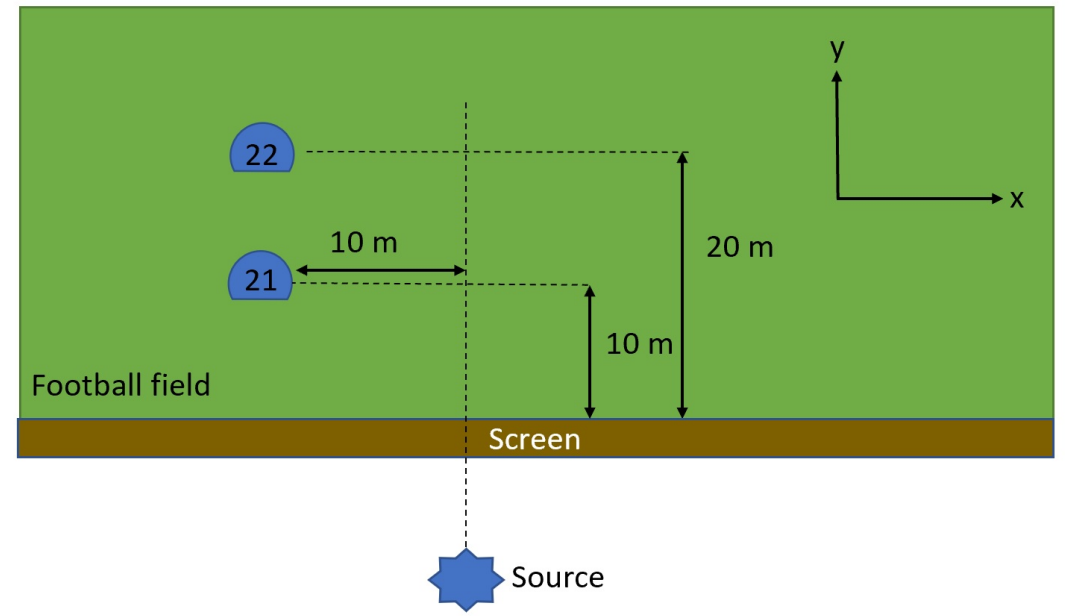

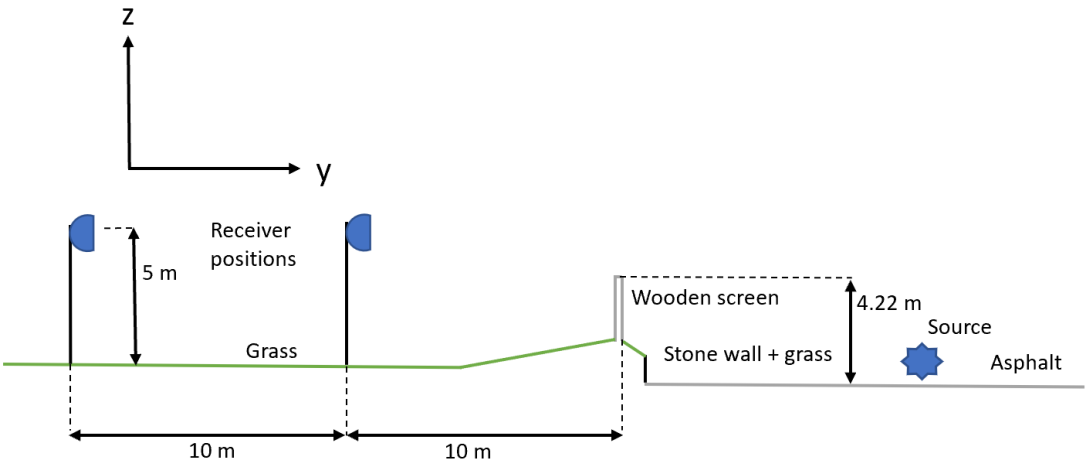

Figure 4.11: Setup highlighting position 21 and 22 at single-edge diffraction measurements with results presented in figure 4.12.

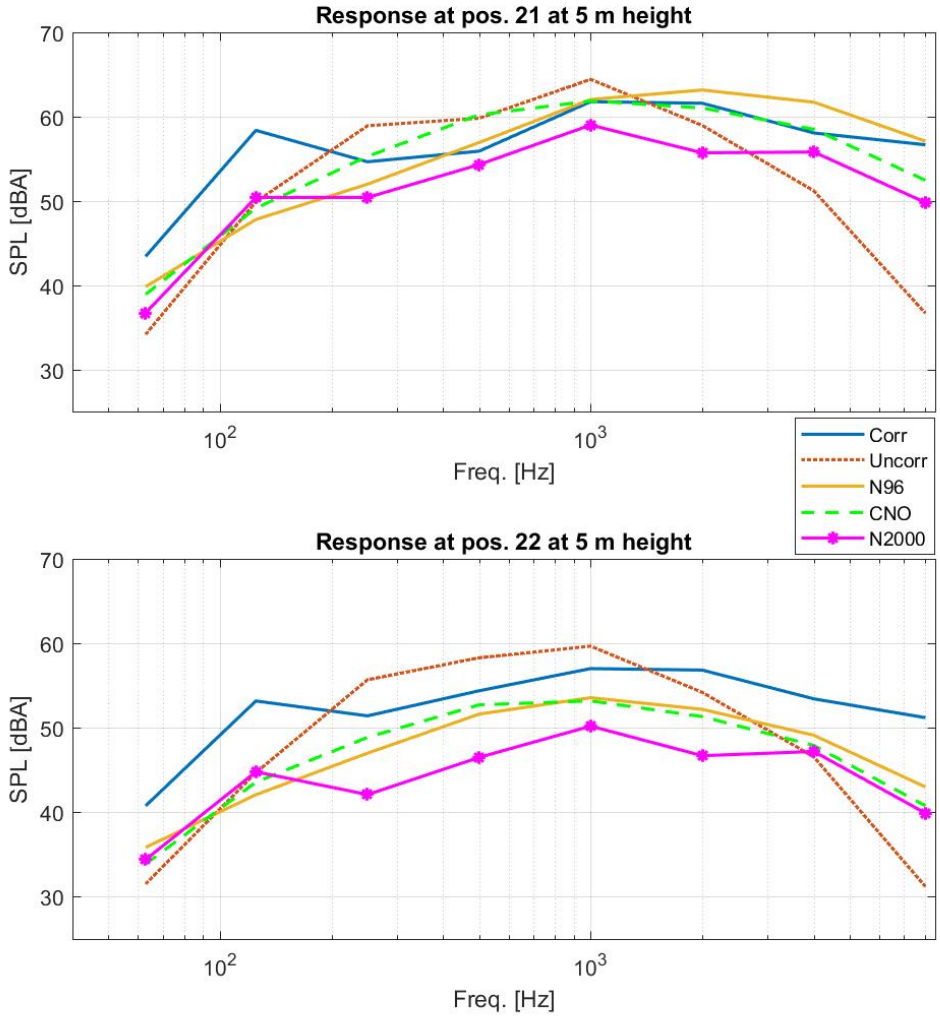

Figure 4.12: SPL of single-edge diffraction measurements showing the corrected speaker (*Corr*), the uncorrected speaker (*Uncorr*), NORD96 (*N96*), CNOSSOS-EU (*CNO*) and NORD2000 (*N2000*).

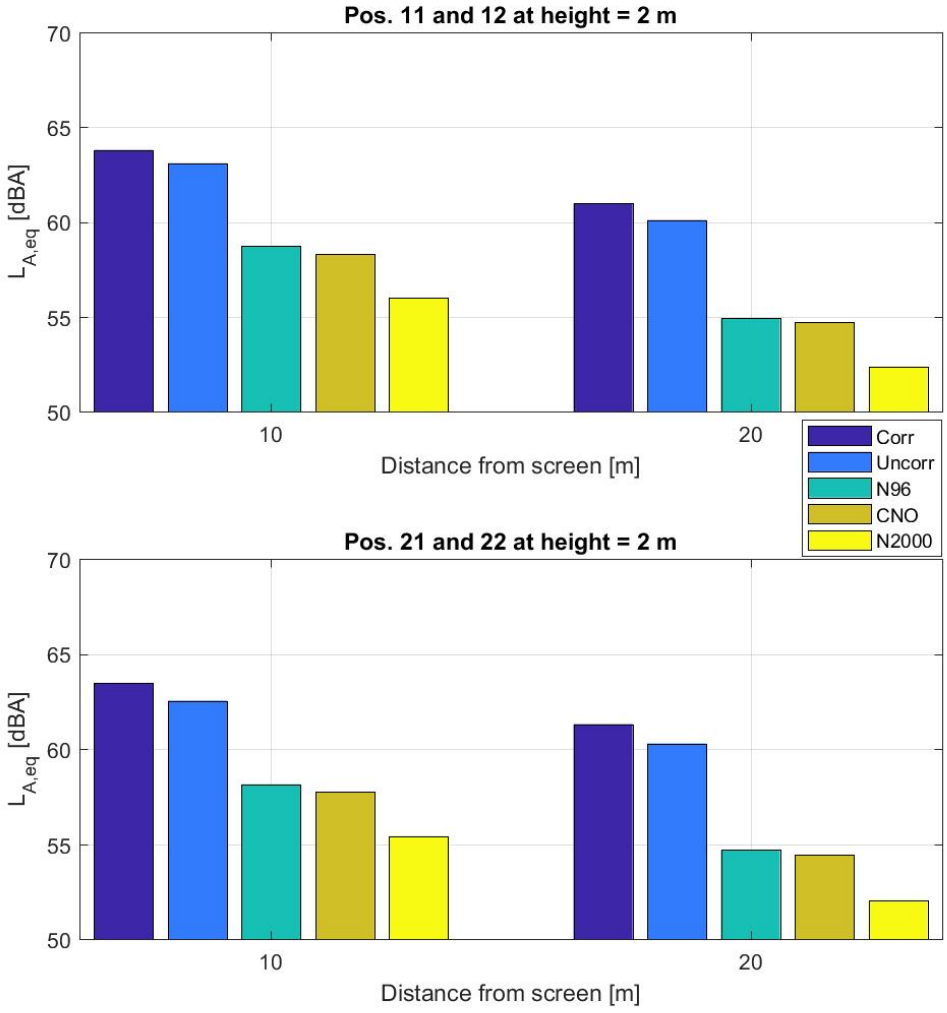

Figure 4.13: $L_{A,eq}$ of single-edge diffraction at 10 and 20 meters from the screen showing the corrected speaker (*Corr*), the uncorrected speaker (*Uncorr*), NORD96 (*N96*), CNOSSOS-EU (*CNO*) and NORD2000 (*N2000*).

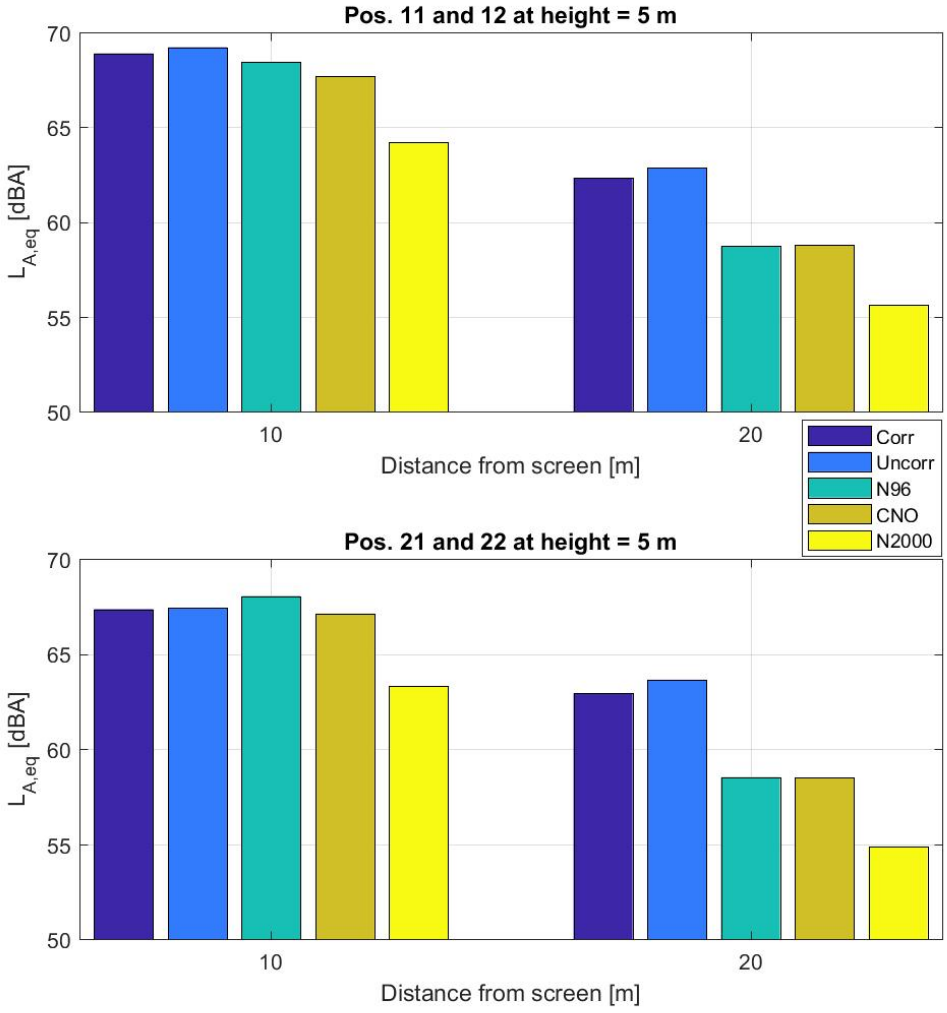

Figure 4.14: $L_{A,eq}$ of single-edge diffraction at 10 and 20 meters from the screen showing the corrected speaker (*Corr*), the uncorrected speaker (*Uncorr*), NORD96 (*N96*), CNOSSOS-EU (*CNO*) and NORD2000 (*N2000*).

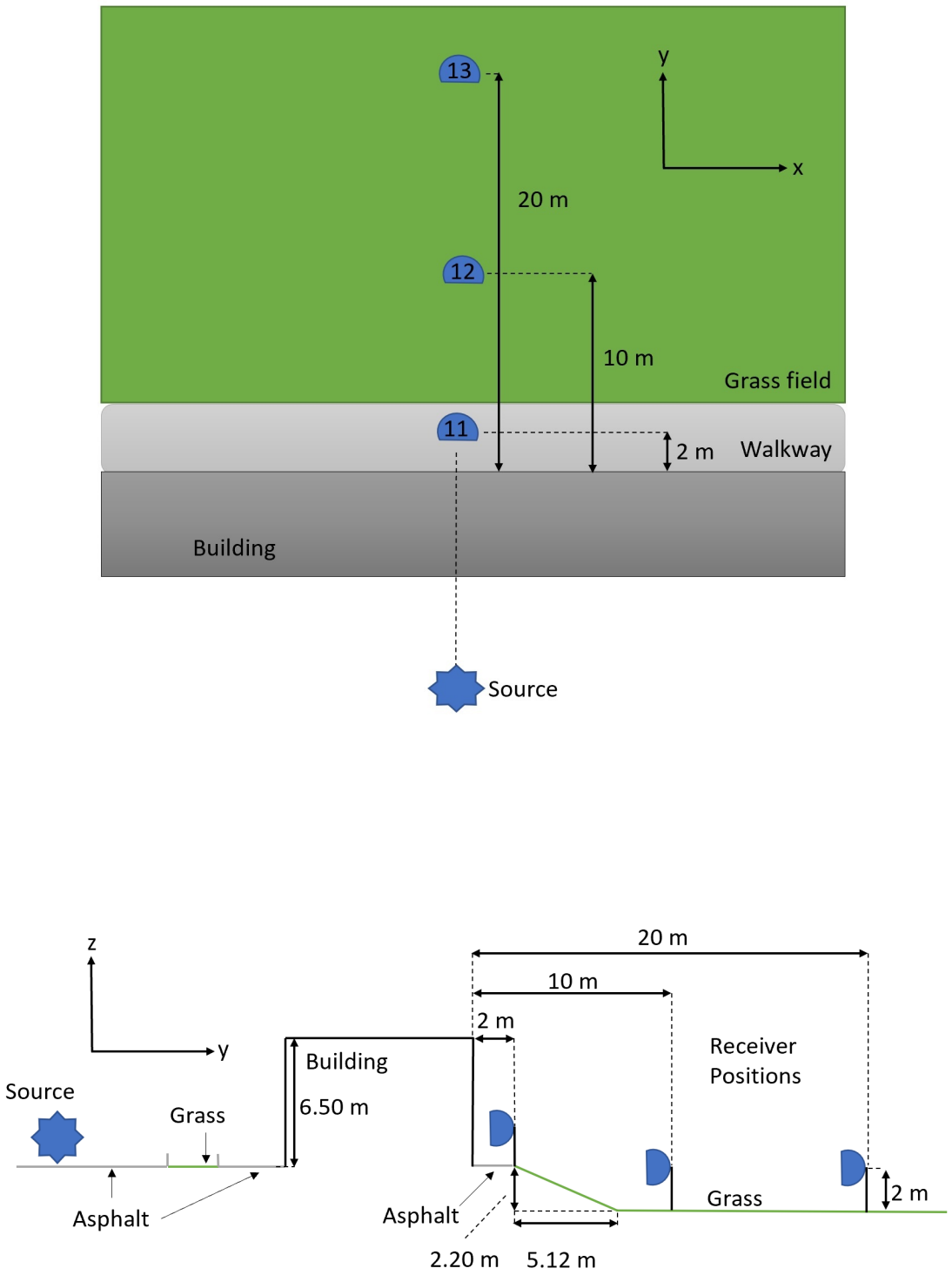

Figure 4.15: Setup highlighting position 11, 12 and 13 at double-edge diffraction measurements with results presented in figure 4.16.

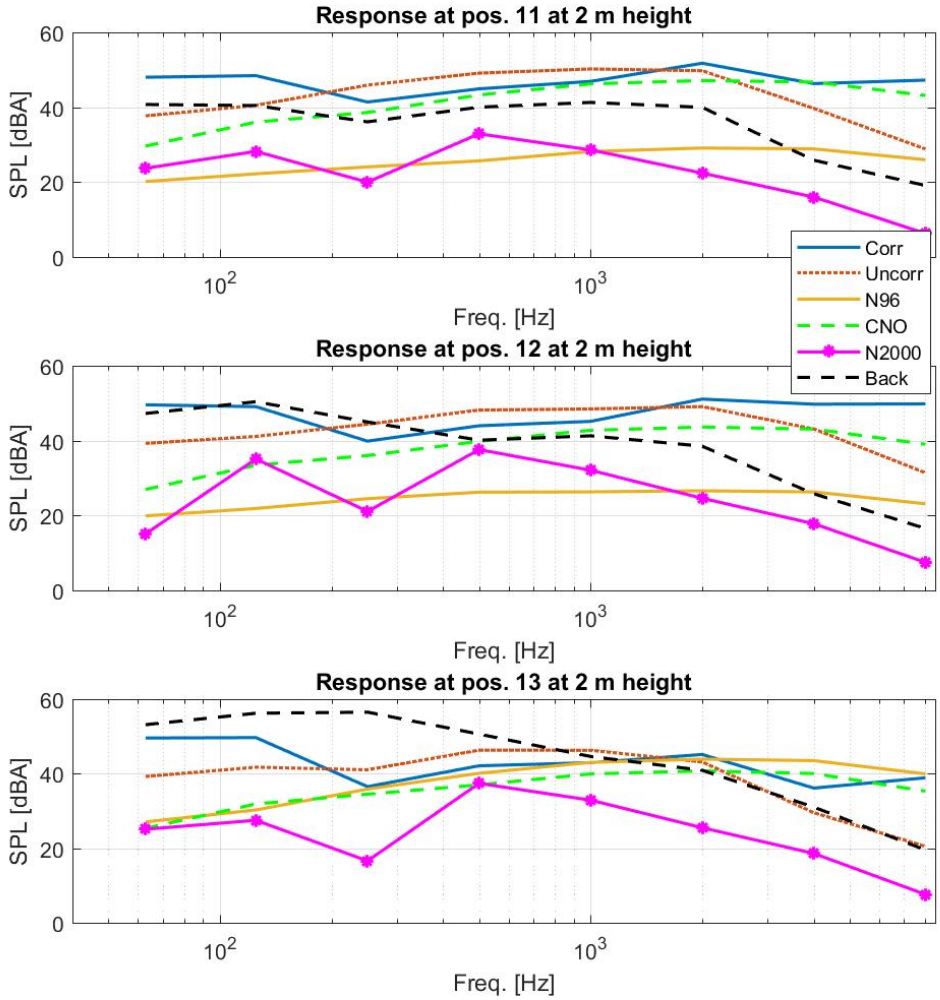

Figure 4.16: SPL of double-edge diffraction measurements showing the corrected speaker (*Corr*), the uncorrected speaker (*Uncorr*), NORD96 (*N96*), CNOSSOS-EU (*CNO*), NORD2000 (*N2000*) and background noise *Back*.

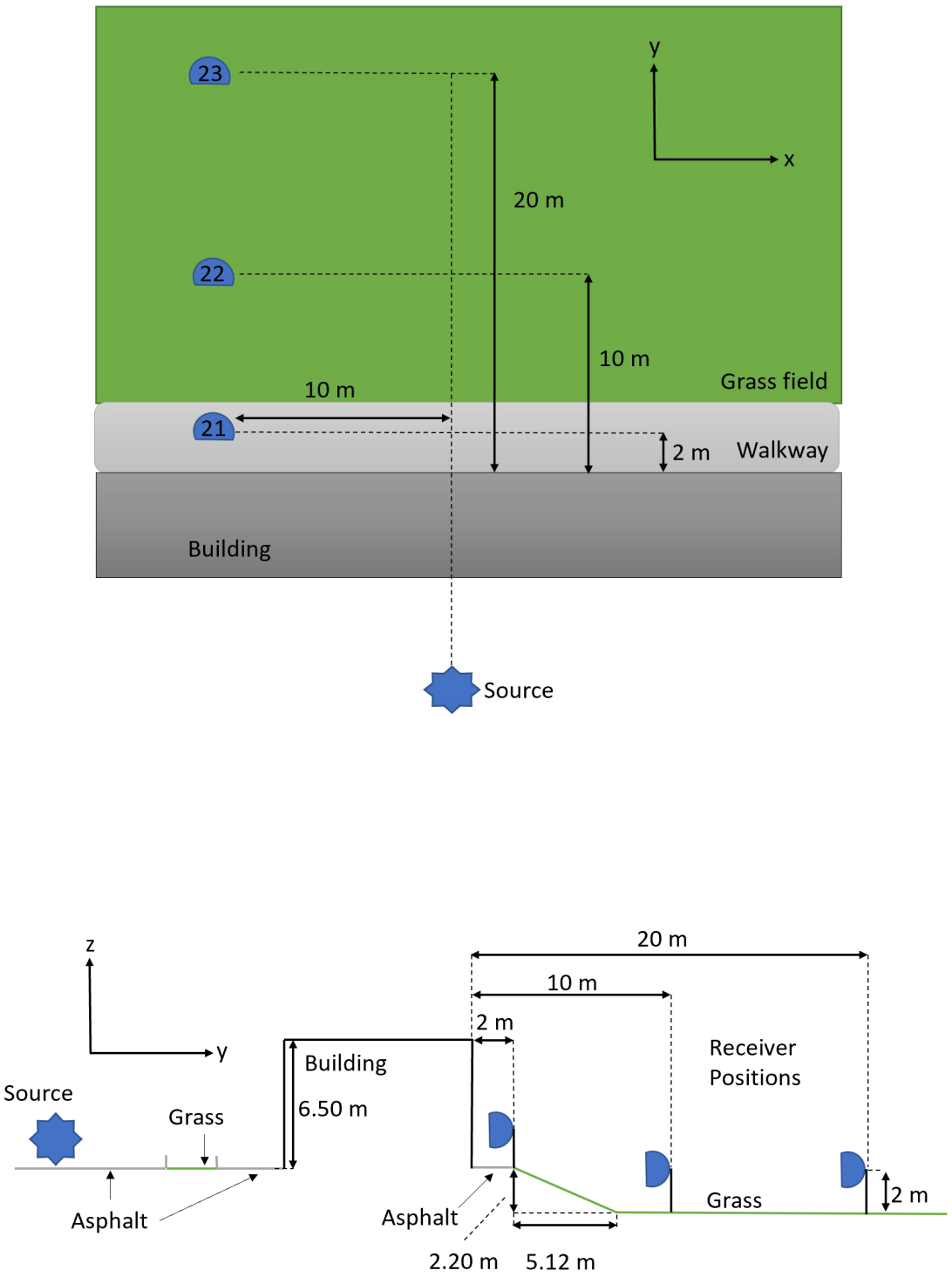

Figure 4.17: Setup highlighting position 11, 12 and 13 at double-edge diffraction measurements with results presented in figure 4.18.

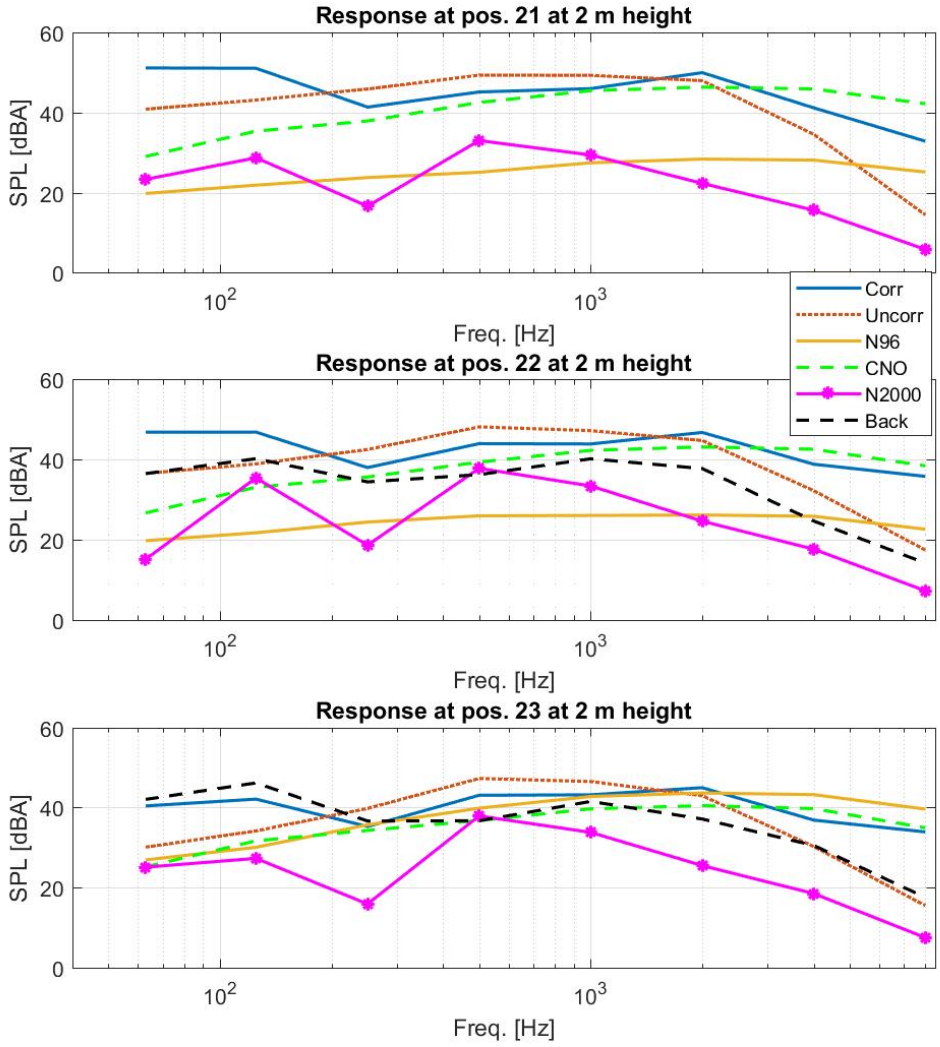

Figure 4.18: SPL of double-edge diffraction measurements showing the corrected speaker (*Corr*), the uncorrected speaker (*Uncorr*), NORD96 (*N96*), CNOSSOS-EU (*CNO*), NORD2000 (*N2000*) and background noise *Back*.

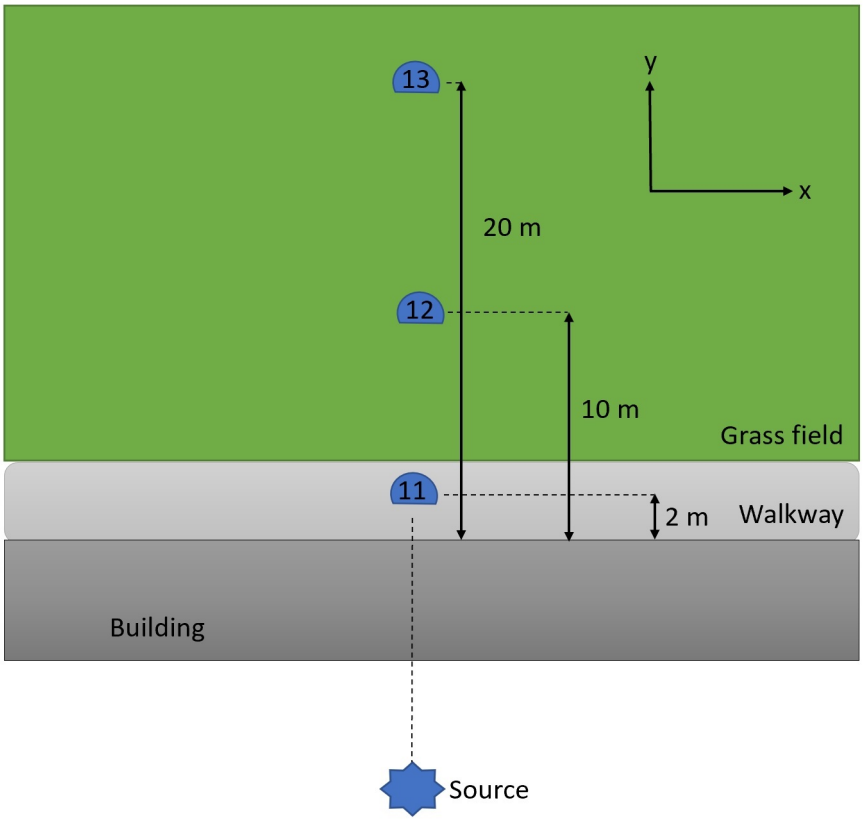

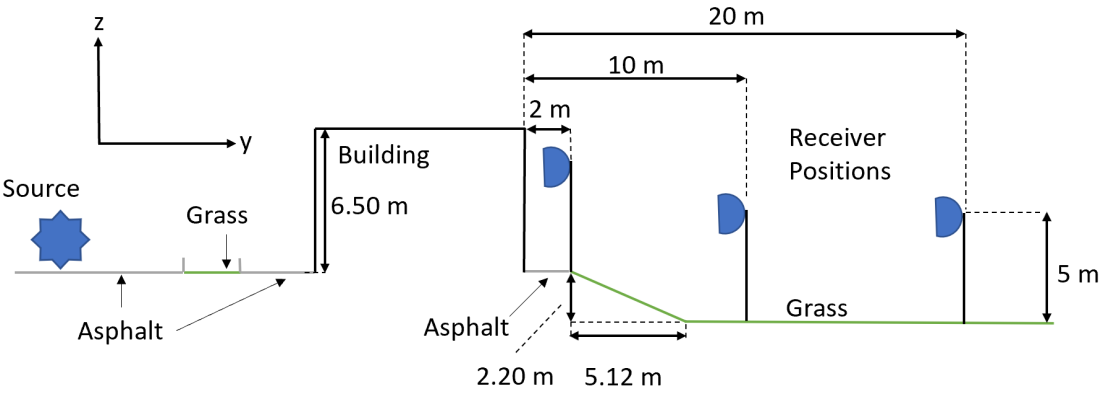

Figure 4.19: Setup highlighting position 11, 12 and 13 at double-edge diffraction measurements with results presented in figure 4.20.

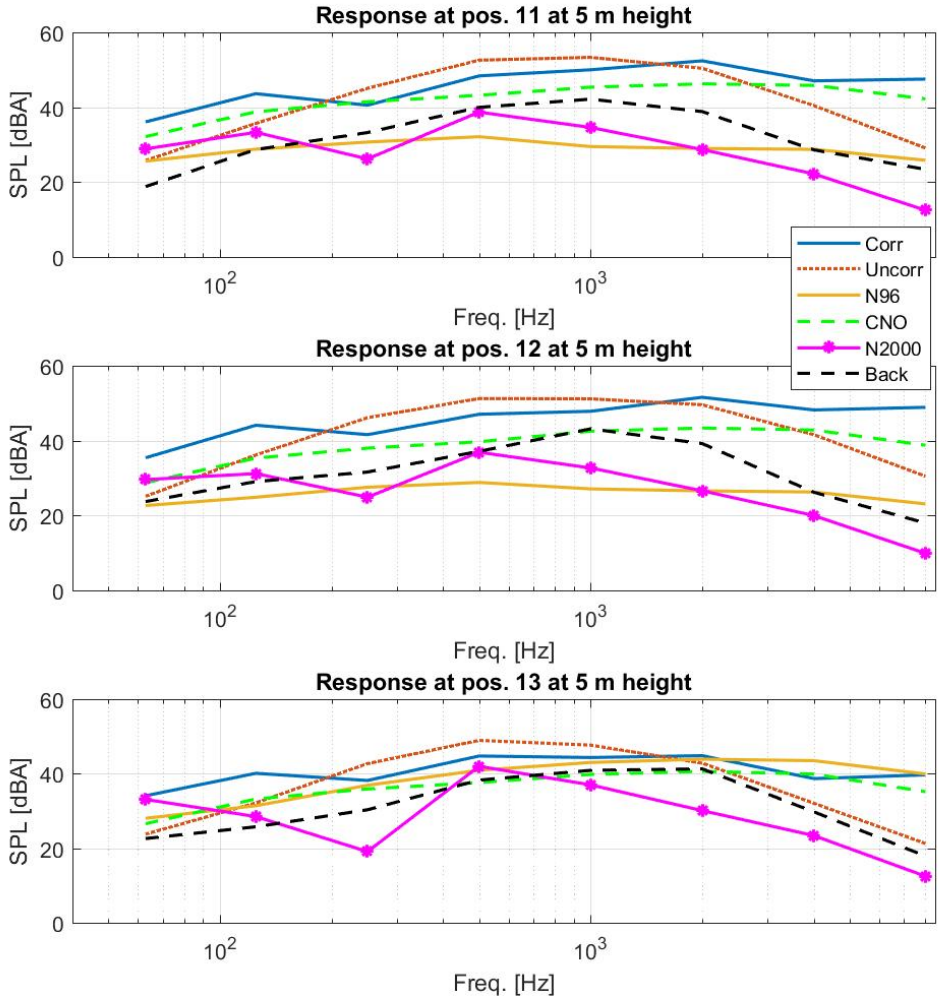

Figure 4.20: SPL of double-edge diffraction measurements showing the corrected speaker (*Corr*), the uncorrected speaker (*Uncorr*), NORD96 (*N96*), CNOSSOS-EU (*CNO*), NORD2000 (*N2000*) and background noise *Back*.

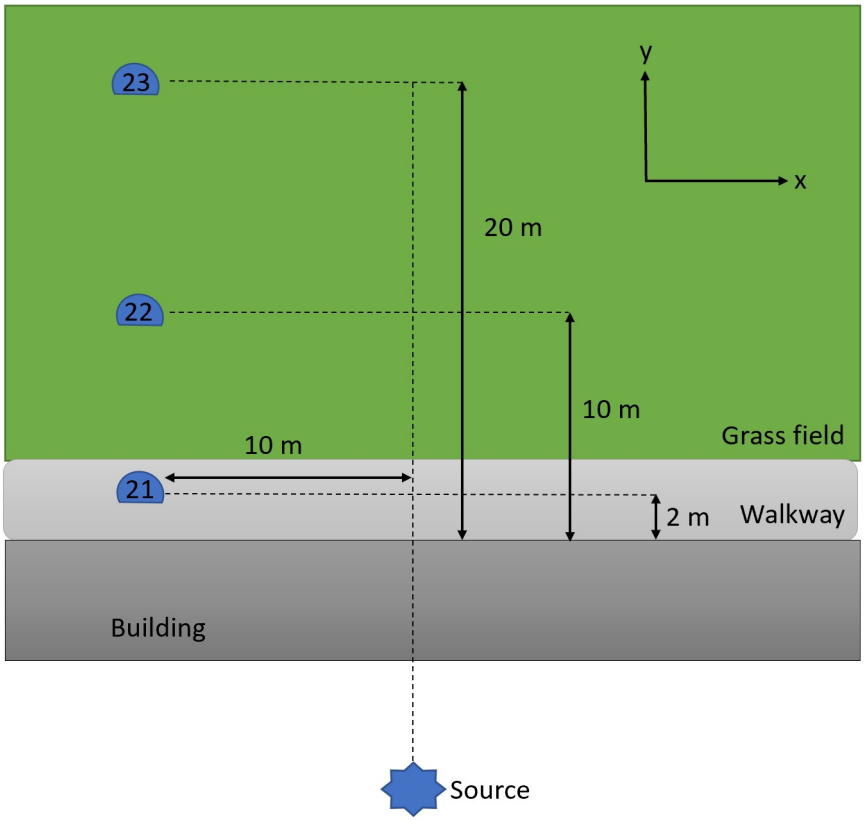

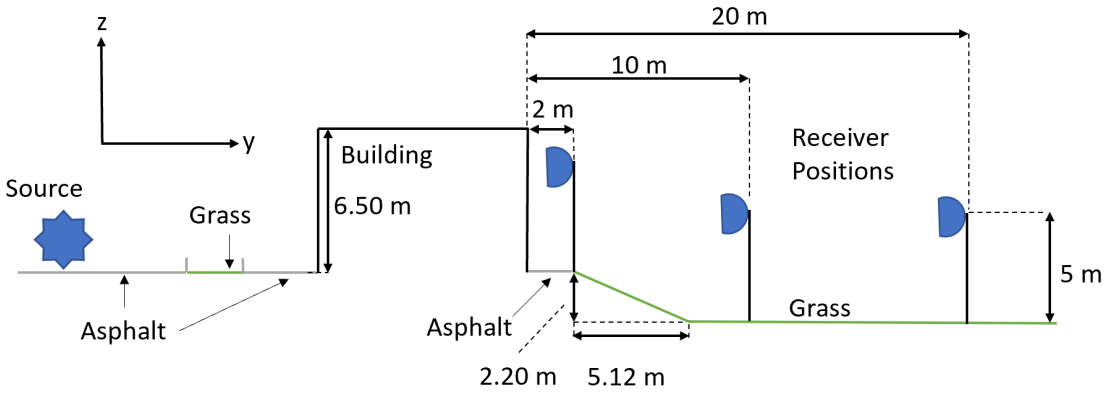

Figure 4.21: Setup highlighting position 11, 12 and 13 at double-edge diffraction measurements with results presented in figure 4.22.

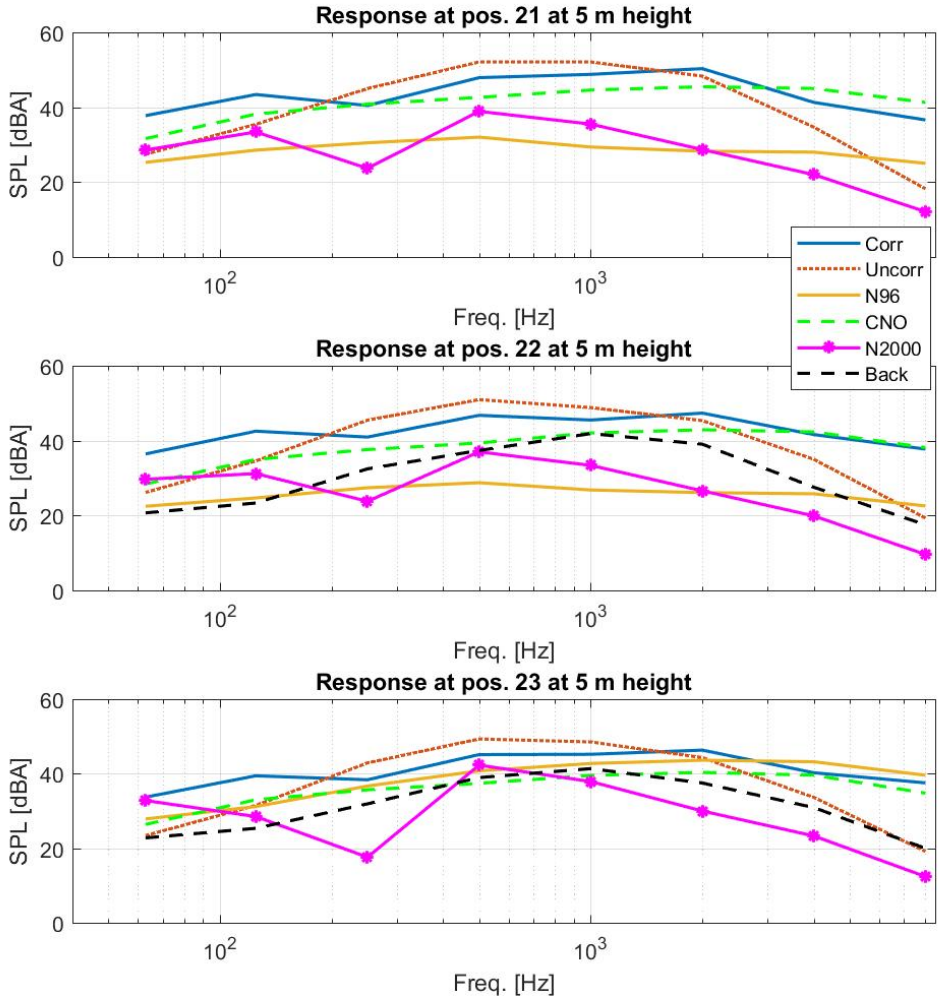

Figure 4.22: SPL of double-edge diffraction measurements showing the corrected speaker (*Corr*), the uncorrected speaker (*Uncorr*), NORD96 (*N96*), CNOSSOS-EU (*CNO*), NORD2000 (*N2000*) and background noise *Back*.

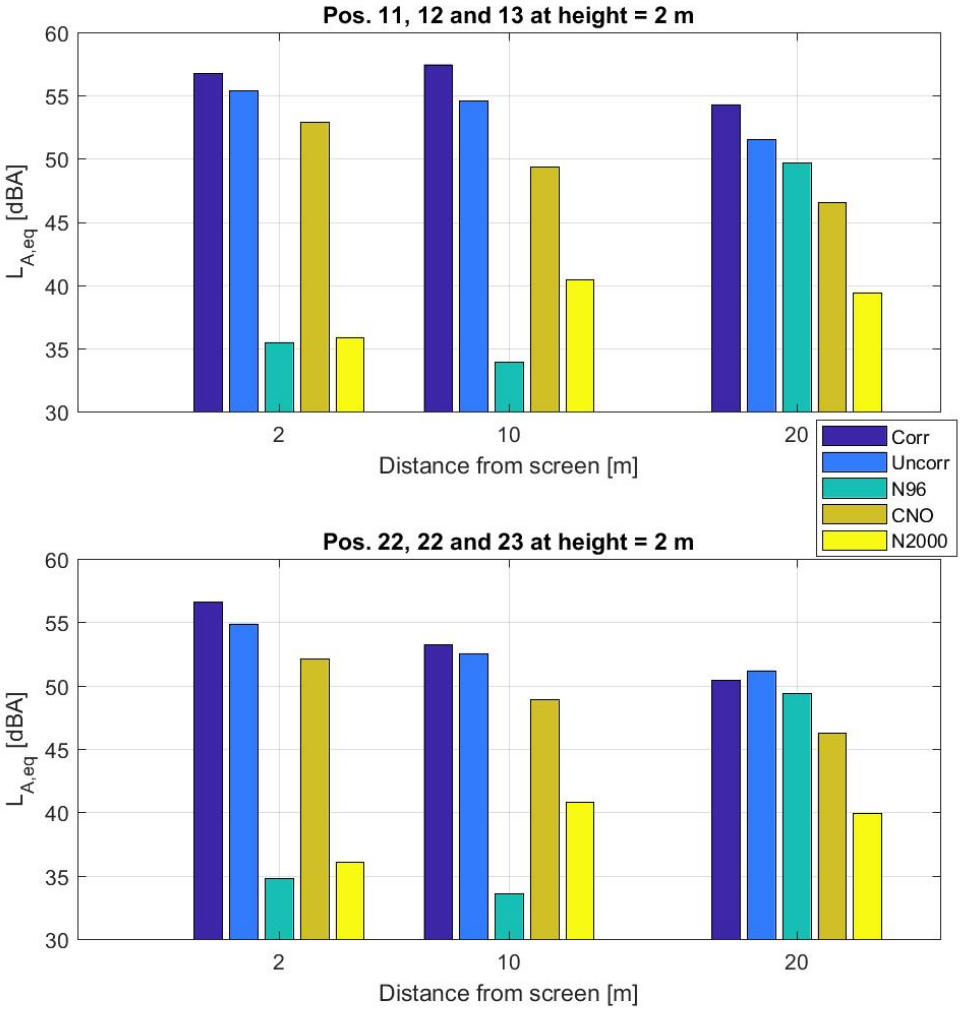

Figure 4.23: $L_{A,eq}$ of double-edge diffraction at 2, 10 and 20 meters from the building showing the corrected speaker (*Corr*), the uncorrected speaker (*Uncorr*), NORD96 (*N96*), CNOSSOS-EU (*CNO*) and NORD2000 (*N2000*).

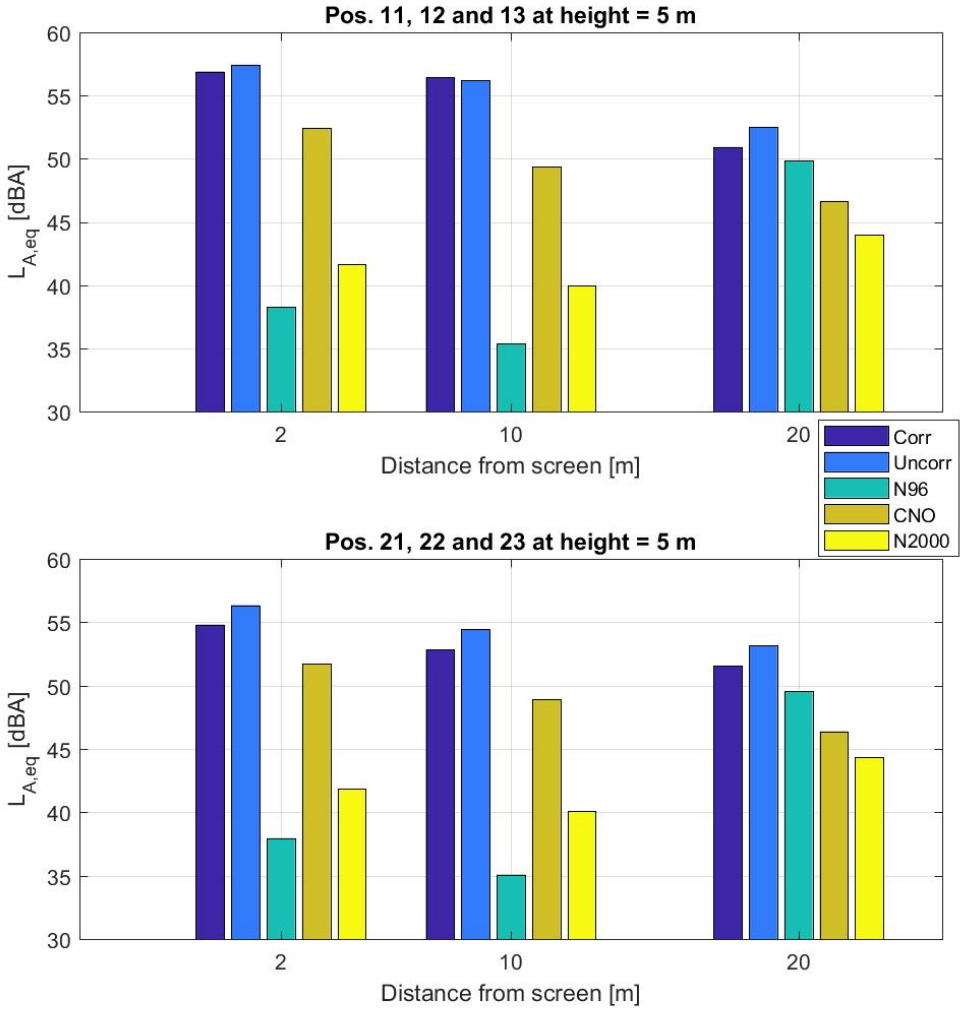

Figure 4.24: $L_{A,eq}$ of double-edge diffraction at 2, 10 and 20 meters from the building showing the corrected speaker (*Corr*), the uncorrected speaker (*Uncorr*), NORD96 (*N96*), CNOSSOS-EU (*CNO*) and NORD2000 (*N2000*).

Chapter 5

Discussion

A correction was added to the speaker to accommodate the fact that it does not reproduce pink noise with equal SPL at all octave bands. Looking at table 4.2, the correction factor is quite significant at 8 kHz, and it is expected to have a significant impact on SPL values, which raises the question if a correction factor should be used. This lead to the decision that both the corrected and uncorrected measurements should be presented and compared to the prediction methods.

5.1 Speaker Calibration

When studying figure 4.1 and 4.2 it is clear that with Δ_{corr} from table 4.2, the speaker SPL is coherent with NORD96 and CNOSSOS-EU, and seem to be quite accurate with NORD2000 at mid to higher frequencies. Though at low frequencies, NORD2000 seem to predict significant damping that might be caused by an early reflection from the ground beneath the speaker, however, since this thesis focuses on diffraction and not on how the different methods model the speaker, this will not be discussed further.

When studying the results from table 4.3 to 4.8, $L_{A,eq}$ should be more or less comparable to ensure that the waves are not significantly attenuated before the barrier diffracts them. So favourably, the difference in $L_{A,eq}$ should not be higher than 1 dBA. Still, in table 4.4, there is a significant difference of 2 dBA in the 5-metre front distance (F2) of the CNOSSOS simulated speaker making it a possible cause of error regarding the accuracy since this impacts the direct ray that is measured. The building configuration is also concerning, when comparing the prediction methods and the measured results in 4.6 to 4.8. Here, all front measurements at 5 metre (F2) are above (NORD96) or below (CNOSSOS-EU and NORD2000) 1 dBA. Meaning that one must have this in mind when comparing the measured SPL to the prediction methods. Some places the side rays give an even higher deviation at approximately 2.5 dB; however, since those have more of an impact on the side reflections, it is assumed that they are not as influential. In general, these results may imply that some attenuations from the environment can have had an impact on the direct rays. From the measurements conducted at the building, it could be explained since the parking lot was occupied by cars at close range of the speaker. However, the speaker at the single screen measurements was far from an object, meaning one can only speculate if the stone wall and the grass hill that the screen stood upon, had any attenuating reflections on the direct line.

5.2 Comparing SPL and $L_{A,eq}$

5.2.1 Single Screen

Comparing the corrected and uncorrected measured SPL in figures 4.6 and 4.8 it is clear that in the low and the high-frequency bands, there are apparent deviations. When comparing the mid frequencies of the uncorrected SPL to the prediction methods, there tends to be a significant gap that is more consistent with the corrected SPL. Looking at the 250 Hz and 500 Hz octave band, the corrected SPL and the prediction methods seems to comply, except for NORD2000 which, to a certain degree, predicts a lower SPL. When studying the corrected measurements at the low-frequency octave bands, there is a significant high SPL of about 55 dBA at 125 Hz, of which might be explained by background noise affecting the measurements or the quality of the screen itself. At high frequencies, the high response might be caused by the fact that the screen has some significant leakages. Having in mind that the prediction method assumes a robust and dense screen substantiates the argument that the physical screen used in these measurements did not, to a certain degree, give sufficient diffraction that is needed for retrieving more reliable measurements. The uncorrected SPL does not seem to detect this behaviour. A repeating pattern at almost fall figures occurs between the prediction methods where NORD96 and CNOSSOS-EU predicts a corresponding SPL at low to mid frequencies, but deviate slightly at higher frequencies where CNOSSOS-EU and NORD2000 seem to predict the same SPL.

Studying figures 4.14 and 4.12 where there is less influence from the screen is, the uncorrected SPL seems to be consistent with predicted methods; however, at higher frequencies, the damping is significantly underestimated suspecting the SPL at these levels are close to the background noise levels. The corrected SPL shows the same high SPL at 125 Hz, still at about 60 dB, strengthening the assumption that it the uncorrected speaker does not emit high enough levels at these areas and what is measured is background noise. As there is less diffraction at this height, the prediction methods seem to be more accurate. Both NORD96 and CNOSSOS-EU seem to be consistent with the corrected measurements. Especially CNOSSOS-EU seems to be accurate at a 10-metre distance. NORD2000 still have some discrepancies at mid frequencies when compared to the other prediction methods, but seem to be more compliant

NORD2000 predicts an SPL that is generally lower, however, when compared to the corrected measurements in figure 4.12, there seems to be a resemblance in the curve behaviour, although this may be a random occurrence.

The measured equivalent sound levels $L_{A,eq}$ as seen in figures 4.13 and 4.14, further asserts that the screen was not optimal for measuring diffraction as presented in the bar charts at 2 metre height indicates a clear difference between measurements and prediction methods in $L_{A,eq}$ of at least 5 dBA. Only at the height of 5 metres at a distance of 10 meters, the measurements and prediction methods seem to match each other; however, at 20 meters $L_{A,eq}$ is lower. It might be explained by the measurement positions being located further within the shadow area, thus being more affected by diffracted waves that have been reflected by the ground.

NORD96 and CNOSSOS-EU have similar SPL; hence, the predicted $L_{A,eq}$ are quite the same. Also, as mentioned previously, CNOSSOS-EU has $L_{A,eq}$ that is two dBA lower than the noise source, which may imply that CNOSSOS-EU might predict a slightly higher level in general.

Since NORD2000 generally predicts a lower SPL, the $L_{A,eq}$ is lower compared with the other prediction methods.

5.2.2 Building

When studying figures 4.16 and 4.18, it is some unexpected results form the background noise, especially at low frequencies. It is not common to experience background noise levels that

are higher than the measured SPL, which might lead to the conclusion that this could have been caused by an unwanted environmental noise source, maybe due to the air-condition or an arbitrary car passing by. It does not seem to be the same case at figures 4.20 4.22 where the background noise levels are consistently below both the corrected and uncorrected measurements. The reason for this difference in background noise measurements is not known; however, the background noise levels at 5-meter height seem to be what one would expect from an open area away from any significant unwanted noise pollution altering the measurements.

Comparing the SPL of the corrected and uncorrected measurements in figure 4.18, it is clear that the corrected measurements are more consistent with the background noise at low to mid-frequency bands. However, the uncorrected measurement seems more precise at higher frequencies at 20 meters, which is interesting since, in figure 4.16, the SPL of the corrected measurements seem flat or even increasing at higher frequencies. It is unexpected since the SPL tend to have more of a roll-off from mid to high frequencies.

Except for low frequencies, CNOSSOS-EU seems to be the most accurate prediction method for double diffraction. NORD96 predicts damping from the diffraction that is significantly low both at 2 and 10 meters but becomes more accurate at 20 meters where the diffraction might not have significant influence. Also, to predict a low SPL in general, NORD2000 computes damping at the 250 Hz octave band before giving a considerable roll-off from 500 Hz to 8 kHz. The corrected measurement also seems to include damping at 250 Hz although not as high as NORD2000. NORD2000 tend to be more accurate at 20 metres (pos. 13 and 23); however, it does not seem to be a clear roll-off that is comparable with any of corrected measurements.

Results presented in figures 4.20 and 4.22 seems to deem CNOSSOS-EU as the most accurate method at 2 and 10-metre distance. Again, NORD96 predicts a low SPL at 2 and 10 metres and becomes more precise at 20 meters. The same damping and roll-off is prominent in NORD2000, as well as predicting lower SPL in general when compared to the corrected measurements. Keep in mind that the measurements between 2 and 10 metre had a steep grass hill, as shown in figure 4.19, meaning that the measurements at 5-meter height are not on the same ground level.

Studying figures 4.23 and 4.24, it is evident that NORD96 predicts a $L_{A,eq}$ that is significantly lower than corrected measurements with a discrepancy around 15-25 dBA at 2 and 10 meters, of which one might argue that the prediction method is not applicable for such measurements. At the same distances, NORD2000 predicts a slightly better equivalent sound level, but still, it is not sufficiently accurate. CNOSSOS-EU predicts $L_{A,eq}$ more accurately except at 20 meter where NORD96 is closer to the corrected measurements. For $L_{A,eq}$ of the corrected measurements, it seems that the high SPL at low frequencies probably caused by background noise has a discrepancy of 5-8 dBA when compared to CNOSSOS-EU. As discussed previously, the speaker modelled in CNOSSOS-EU has a lower $L_{A,eq}$ than the measured speaker at the front (F2) of 1.4 dBA. Correcting for this might lead to a lower discrepancy between the prediction method and the corrected results.

5.3 Main Differences Between Prediction Methods

When comparing NORD96 and CNOSSOS-EU and how they compute single diffraction is very similar. Both evaluate diffraction by one edge with methods using a form of path difference, and both have empirical approaches for finding the ground attenuation. The main difference is when NORD96 seems to have a prediction of the ground attenuation as purely empirical, CNOSSOS-EU uses the image-source method to find the attenuation of the reflected paths and weight these with the ground factor as shown in eq. 2.19 and 2.20. The simulated results seem to affirm this where there are small differences at 2 meter where they mostly have discrepancies

at higher frequencies.

When it comes to double diffraction, the results seem to suggest that NORD96 prediction method is very inaccurate at a close distance from the double-edged barrier. On the contrary, the results deem the prediction from CNOSSOS-EU to be the most accurate, which might imply that the image-source method predicts more accurately attenuation from the ground. It will raise the question of why NORD2000 that has the same way of predicting the reflected rays computes results with such large discrepancy from measured results. Though one can argue to some extent that NORD2000 might be better to predict the behaviour of the SPL curve, it overestimates the damping coefficient and retrieves a lower SPL in general. NORD2000 is very different from other prediction methods. Instead of choosing a ground coefficient G which is a pre-defined value based on empirical results, the ground impedance is determined and given as a complex value indicating a more direct consideration of the phase. What this means, is that it might be possible to predict a better ground attenuation since the predicted topography becomes more complex, giving the user more parameters to determine. As mentioned in chapter 2.7.1, the impedance is determined by the Delany-Bazely impedance model. According to [6], this model works well for most ground surfaces; however, for some essential surfaces like porous asphalt, the method is said to work less well.

5.4 Further Work

It is hard to evaluate ground impedance. Fuchs defines ground as a passive absorber [19] which depends on three main components; porosity, the structure factor and specific flow resistance. Further work might be to do a mapping of the ground surface where these three parameters are estimated and applied in the prediction method. Also, further work might be to find a better screen that is more solid and dense to ensure that the measured SPL is more consistent at higher frequencies. Also, redoing some of the measurements from the building and compare them with these results to ensure that the high SPL at high frequencies is consistent and not a result of disruptive sound from unwanted noise sources. Also, a new background measurement should be conducted to retrieve noise levels that might be more reliable.

Chapter 6

Conclusion

The overall purpose of this thesis was to compare three different prediction methods and evaluate the precision and reliability with the focus on single-edge and double-edge diffraction. Field measurements in ideal locations were conducted and compared to calculations from NORD96, CNOSSOS-EU and NORD2000.

A wooden screen and a solid rectangular building were chosen for the single-edge and double-edge measurements, respectively. The field measurements were conducted in optimal conditions where attenuations from meteorological conditions appeared to be negligible. Meteorological data was not measured at sight but were collected from weather stations closest to the locations. Pink noise was emitted from the source, and two measurements at different heights were conducted at each measurement position. As the speaker did not emit pink noise precisely at all octave bands, a correction was added to encounter this inaccuracy by measuring the speaker in the near-field. The topography was mapped and implemented in SoundPlan 8.0, which did the necessary calculations for all the prediction methods. Post-processing was carried out in Matlab R2017a.

The results from the single-edge measurements show that when compared to the prediction methods both NORD96 and CNOSSOS-EU seem accurate, and NORD2000 seems to overestimate the damping predicting a lower sound pressure level at areas where diffraction are prominent. Also, the wooden screen was not optimal since it had clear signs of degradation with some cracks that can have an impact on the results.

The double-edge measurements gave results that deemed CNOSSOS-EU to be most accurate close to the barrier only outperformed by NORD96 at 20 meters. Close to the barrier, NORD96 predicted a sound pressure level that had high discrepancy when compared to the measurement, and although NORD2000 seem to outperform NORD96 at 2 and 10 meters, CNOSSOS-EU is overall the most reliable prediction method.

A possible explanation for such results is that NORD2000 have many input parameters which include ground impedance. Although that has the potential to map the topography more precisely, it might also lead to wrong predictions if the input parameters are not accurate. The ground impedance parameters might be measured to give a better understanding of the ground reflections involved.

Preferably, further analysis and more measurements must be conducted to confidently determine which model predicts sound pressure level attenuated by diffraction. Finding another location for the single-edge diffraction predictions where the screen has more optimal characteristics might retrieve more reliable results. Also, research involving estimation of the ground impedance might give a more accurate comparison between prediction methods and field measurements.

Bibliography

[1] Demian Halperin. "Environmental Noise and sleep disturbances: A threat to health". In: *Sleep Sci.* 7.4 (2014), pp. 209–212. DOI: 10.1016/j.slsci.2014.11.003.

[2] J. H. Rindel. *Course 85309 - Room acoustic engineering*. Geilo, Norway: Norske Sivilingeniørers Forening (NIF), 1988.

[3] Department of Climate and Environment. "Retningslinje for behandling av støy i arealplanlegging (T1442-2016)". In: (2017).

[4] Miljøminesteriet. "Vejledning fra Miljøstyrelsen - Beregning af ekstern støj fra virksomheder". In: 5 (1993).

[5] "COMMISION DIRECTIVE (EU) No 2015/996 of 19 may 2015 establishing common noise assessement methods according to Directive 2002/49/EC of the European Perlament and of the Council". In: *OJ* L 168 ().

[6] DELTA. "Proposal for Nordtest Method: Nord2000 - Prediction of Outdoor Sound Propagation". In: ().

[7] Thomas D. Rossing, Richard F. Moore, and Paul A. Wheeler. *The Science of Sound*. Pearson, 2002. Chap. 6, pp. 103–121.

[8] Tor Erik Vigran. *Building Acoustics*. Taylor & Francis, 2008. Chap. 3.3, pp. 61–63.

[9] J. B. Allen and D. A. Berkley. "Image method for efficiently simulating small-room acoustics." In: *J. Acoust. Soc. Am.* 65 (1979), pp. 943–950.

[10] Allan Pierce and W. James Hadden. "Sound Diffraction around screens and wedges for arbitrary point source locations". In: *Journal of Acoustic Society of America* 69 (1981).

[11] M. Delany and E. Bazley. "Acoustical properties of fibrous absorbent materials". In: *Applies Acoustics* 49.7 (1970), pp. 1253–1272.

[12] IEC. "IEC 61672-1:2013 Electroacoustics - Sound level meters - Part 1: Specifications". In: (2013).

[13] Qsources. *Qohm homepage*. 2019. URL: https://www.qsources.be/infra-qsources/qohm/.

[14] NORSONIC. *NOR-280 Product Data sheet*. 2019. URL: https://wpstatic.idium.no/web2.norsonic.com/2016/11/PD-280-Ed1Rev2-En-1116.pdf.

[15] NORSONIC. *NOR-1220 Datasheet*. 2019. URL: http://norsonic.asia/wp-content/uploads/2015/04/Norsonic-Microphones-Datasheet.pdf.

[16] NORSONIC. *NOR-1201 Datasheet*. 2019. URL: http://norsonic.asia/wp-content/uploads/2015/04/Nor1201-Preamplifier.pdf.

[17] NORSONIC. *NOR-1225 Datasheet*. 2019. URL: http://norsonic.asia/wp-content/uploads/2015/04/Norsonic-Microphones-Datasheet.pdf.

[18] NORSONIC. *NOR-1209 Datasheet*. 2019. URL: https://wpstatic.idium.no/web2.norsonic.com/2016/11/PD-1209-Ed1Rev1-Eng-0914.pdf.

[19] H. V. Fuchs. *Applied Acoustics: Consepts, Absorbers and Silencers for Acoustical Comfort and Noise Control*. Springer-Verlag, 2013. Chap. 4, pp. 31–41.

Appendix A

Calculus

A.1 Further Calculus from CNOSSOS-EU

$$C'' = \frac{1 + (5\lambda/e)^2}{1/3 + (5\lambda/e)^2} \tag{A.1}$$

e in eq. A.1 is the direct line between obstacle edges.

$$w = 0.0185 \frac{f_m^{2.5} G_w^{2.6}}{f_m^{1.5} G_w^{2.6} + 1.3 \cdot 10^3 f_m^{0.75} G_w^{1.3} + 1.16 \cdot 10^6} \tag{A.2}$$

$$C_f = d_p \frac{103 w d_p e^{-\sqrt{w d_p}}}{1 + w d_p} \tag{A.3}$$

Table A.1: Choosing generic notations G_w and G_m

	Homogenous conditions			Favourable conditions		
	A_{ground}	$\Delta_{ground,SO}$	$\Delta_{ground,OR}$	A_{ground}	$\Delta_{ground,SO}$	$\Delta_{ground,OR}$
G_w	G'_{path}		G_{path}			
G_m	G'_{path}		G_{path}	G'_{path}		G_{path}

Appendix B

Ground effect

1/1 oktav f_c [Hz]	$\Delta L_{g,s}$ eller $\Delta L_{g,i}$ [dB]	$\Delta L_{g,c}$ [dB]
63	1.5	3 m [5]
125	1.5 - G · a(h) [1]	3 m(1 - G_c) [5]
250	1.5 - G · b(h) [2]	
500	1.5 - G · c(h) [3]	
1000	1.5 - G · d(h) [4]	
2000	1.5 (1 - G)	
4000	1.5 (1 - G)	
8000	1.5 (1 - G)	

[1] $a(h) = 1.5+3.0 \cdot e^{-0.12(h-5)^2}(1-e^{-\frac{d}{50}})+5.7 \cdot e^{-0.09h^2}(1-e^{-2.8 \cdot 10^{-6} \cdot d^2})$

[2] $b(h) = 1.5+8.6 \cdot e^{-0.09 \cdot h^2}(1-e^{-\frac{d}{50}})$

[3] $c(h) = 1.5+14.0 \cdot e^{-0.46 \cdot h^2}(1-e^{-\frac{d}{50}})$

[4] $d(h) = 1.5+5.0 \cdot e^{-0.9 \cdot h^2}(1-e^{-\frac{d}{50}})$

[5] $m = 0$ når $d \leq 30\,(h_i + h_s)$

$m = 1 - \frac{30\,(h_s + h_i)}{d}$ når $d > 30\,(h_s + h_i)$

Hvis $m < 0$, sættes m lig med nul.

Figure B.1: Table for computing ground attenuation according to NORD96. G = 0 for a hard surface and G = 1 for a porous surface [4].

Description	Type	(kPa · s/m²)	G value
Very soft (snow or moss-like)	A	12,5	1
Soft forest floor (short, dense heather-like or thick moss)	B	31,5	1
Uncompacted, loose ground (turf, grass, loose soil)	C	80	1
Normal uncompacted ground (forest floors, pasture field)	D	200	1
Compacted field and gravel (compacted lawns, park area)	E	500	0,7
Compacted dense ground (gravel road, car park)	F	2 000	0,3
Hard surfaces (most normal asphalt, concrete)	G	20 000	0
Very hard and dense surfaces (dense asphalt, concrete, water)	H	200 000	0

Figure B.2: Table for computing ground factor according to CNOSSOS-EU [5]

Impedance class	Representative flow resistivity σ (kPasm^{-2})	Range of Nordtest flow resistivity classes	Description
A	12.5	10, 16	Very soft (snow or moss-like)
B	31.5	25, 40	Soft forest floor (short, dense heather-like or thick moss)
C	80	63, 100	Uncompacted, loose ground (turf, grass, loose soil)
D	200	160, 250	Normal uncompacted ground (forest floors, pasture field)
E	500	400, 630	Compacted field and gravel (compacted lawns, park area)
F	2000	2000	Compacted dense ground (gravel road, parking lot, ISO 10844)
G	20000	-	Hard surfaces (most normal asphalt, concrete)
H	200000	-	Very hard and dense surfaces (dense asphalt, concrete, water)

Figure B.3: Table for computing ground impedance according to NORD2000 [6]

Roughness class	Representative σ_r	Range of heights
N: Nil	0	±0.25 m
S: Small	0.25 m	±0.5 m
M: Medium	0.5 m	±1 m
L: Large	1 m	±2 m

Figure B.4: Classification of Ground roughness.